The Journal of Neuroscience, May 1992, 12(5): 1977–1999

Quantitative Enzyme Radioautography with ^{3}H-Ro 41-1049 and ^{3}H-Ro 19-6327 *in vitro*: Localization and Abundance of MAO-A and MAO-B in Rat CNS, Peripheral Organs, and Human Brain

J. Saura, R. Kettler, M. Da Prada, and J. G. Richards

F. Hoffmann-La Roche Ltd., Pharma Division, Preclinical Research, CH-4002 Basel, Switzerland

Monoamine oxidases A and B (MAO-A and MAO-B) oxidatively deaminate neurotransmitter and xenobiotic amines. Since the cellular localization of the isoenzymes in the CNS and peripheral organs determines to a large extent which substrate has access to which isoenzyme, knowledge of their tissue distribution and cellular localization is essential. Here we describe how reversible and selective inhibitors of MAO-A and MAO-B [Ro 41-1049 and Ro 19-6327 (lazabemide), respectively] can be used, as tritiated radioligands, to map the distribution and abundance of the enzymes in microscopic regions of the rat CNS and peripheral organs, and human brain by quantitative enzyme radioautography. The *in vitro* binding characteristics of both radiolabeled inhibitors revealed them to be selective, high-affinity ligands for the respective enzymes. K_D and B_{max} values for ^{3}H-Ro 41-1049 in rat cerebral cortex were 10.7 nM and 7.38 pmol/mg protein, respectively, and for ^{3}H-Ro 19-6327 were 18.4 nM and 3.45 pmol/mg protein, respectively. In accordance with their potencies as enzyme inhibitors, binding to MAO-A and MAO-B was competitively inhibited by clorgyline (IC_{50} = 1.4 nM) and L-deprenyl (selegiline; IC_{50} = 8.0 nM), respectively. The capacities of various rat and human tissues to bind the radioligands correlated extremely well with their corresponding enzyme activities. As revealed by the respective binding assays, the distribution and abundance of MAO-A and MAO-B in the tissues investigated differed markedly. MAO-A was most abundant in the locus coeruleus, paraventricular thalamus, bed nucleus of the stria terminalis, median habenular nucleus, ventromedial hypothalamus, raphe nuclei, solitary tract nucleus, inferior olives, interpeduncular nucleus, claustrum, and numerous peripheral tissues, including liver, vas deferens, heart, superior cervical ganglion, and exocrine and endocrine pancreas. In contrast, MAO-B was most abundant in the ependyma, circumventricular organs, olfactory nerve layer, periventricular hypothalamus, cingulum, hippocampal formation, raphe nuclei, paraventricular thalamus, mammillary nuclei, cerebellar Bergmann glia cells, liver, posterior pituitary, renal tubules, and endocrine pancreas.

The cellular localization of the isoenzymes in both rat and human brain differs markedly and does not reflect the distribution of the presumed natural substrates, for example, absence of MAO-A in serotoninergic neurons. Indeed, the present evidence suggests that, whereas MAO-A is found in noradrenergic and adrenergic neurons, MAO-B occurs in astrocytes, serotoninergic neurons, as well as ventricular cells, including most circumventricular organs. The physiological roles of the enzymes are discussed in the light of these findings, some of which were unexpected.

Possible roles of MAO-A and MAO-B in the etiology of depression, Parkinson's disease, and Alzheimer's disease might be elucidated by studying their distribution and regulation in diseased, postmortem human brain using this selective, quantitative, and high-resolution technique.

Monoamine oxidases (EC 1.4.3.4.; MAO) are flavoproteins—integral to outer mitochondrial membranes of neurons, glia, and other cells—that oxidatively deaminate neurotransmitter and xenobiotic amines (Blaschko et al., 1937; Youdim et al., 1988; Haefely et al., 1992). The enzyme exists in two forms, MAO-A and MAO-B, which are identified by their inhibitor sensitivity and by their substrate selectivity (Johnston, 1968; Knoll and Magyar, 1972; for reviews, see Denney and Denney, 1985; Dostert et al., 1989; Youdim and Finberg, 1990). In rodent brain, 5-HT, dopamine, and noradrenaline are preferentially metabolized by MAO-A; the trace amines phenethylamine and methylhistamine, by MAO-B; and tyramine as well as octopamine, by both enzymes. In human brain, a similar specificity prevails except that dopamine is a substrate for both enzymes.

MAO-A and MAO-B inhibitors have therapeutic potential for the treatment of depression, Parkinson's disease, and perhaps Alzheimer's disease. The use of reversible inhibitors of MAO-A for the treatment of depression (Burkard et al., 1989; Da Prada et al., 1989a,b, 1990a; Haefely et al., 1992) has received renewed impetus from clinical findings with the novel MAO-A inhibitors moclobemide and brofaromine. Moreover, the potential of MAO-B inhibitors for the treatment of Parkinson's disease has gained credence from a multicenter clinical study showing that L-deprenyl (selegiline) is able to delay the necessity for L-dopa therapy (Parkinson study group, 1989a,b; Tetrud and Langston, 1989; Heikkila et al., 1990). The recent discovery of a novel class of highly selective, mechanism-based, and reversible inhibitors of MAO-A (Ro 41-1049) and MAO-B [Ro 19-6327 (lazabemide), currently in phase II clinical trials for Parkinsonism] provided research tools to investigate the molecular mechanisms of enzyme–inhibitor interactions (Ce-

Received May 22, 1991; revised Sept. 27, 1991; accepted Jan. 17, 1992.

We are grateful to Professor Willy Haefely and Dr. Andrea Cesura for helpful discussions, Mr. Roland Krauer for photography, and Mrs. Martine Wdonwicki for typing the manuscript.

Correspondence should be addressed to Dr. Grayson Richards, F. Hoffmann-La Roche Ltd., Pharma Division, Preclinical Research, Building 69, Room 234, CH-4002 Basel, Switzerland.

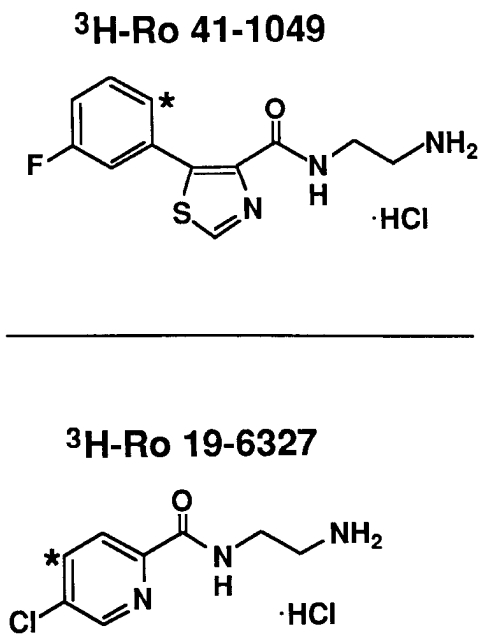

Figure 1. Chemical structures of the tritiated (*) inhibitors of MAO-A and MAO-B, Ro 41-1049 and Ro 19-6327, respectively, used in the present study.

sura et al., 1989, 1990). Recently, research on the physiological and pathological roles of MAO-A and MAO-B in health and disease has been further accelerated by the purification and molecular cloning of the human enzymes (Bach et al., 1988; Grimsby et al., 1991; for review, see Abel et al., 1988) and rat enzymes (Ito et al., 1988; Kuwahara et al., 1990).

The physiological roles of the isoenzymes are twofold: to facilitate indirectly the inactivation of released neurotransmitter amines, and to act as scavengers preventing various natural substrates from accumulating in monoaminergic neurons to act as false transmitters. Since the cellular localization of MAO-A and MAO-B in the CNS and peripheral organs determines to a large extent which substrate has access to which isoenzyme, knowledge of the tissue distribution and cellular localization of the enzymes is essential.

Efforts to determine the cellular localization and abundance of the enzymes have, to date, relied on enzyme histochemical and immunohistochemical investigations (Glenner et al., 1957; Graham and Karnovsky, 1965; Levitt et al., 1982; Westlund et al., 1985, 1988; Arai et al., 1986; Thorpe et al., 1987; Konradi et al., 1988, 1989; Kirchgessner and Pintar, 1991). Although these techniques have revealed the cellular localization of MAO-A and MAO-B, enzyme radioautography using radiolabeled inhibitors as high-affinity substrates offers a highly sensitive and quantitative assay to determine the distribution and abundance of the enzymes in tissue sections of discrete regions of the CNS and peripheral organs. The present study describes the binding characteristics and tissue distribution of ^{3}H-Ro 41-1049 and ^{3}H-Ro 19-6327 (which are highly selective, reversible inhibitors of MAO-A and MAO-B, respectively) (Richards et al., 1988, 1992; Kettler and Da Prada, 1989; Kettler et al., 1989; Haefely et al., 1990; Saura Marti et al., 1990a,b).

Materials and Methods

Tissue preparation. Male Fü albino rats (specific pathogen free) weighing ~120 gm, housed under a controlled light/dark cycle and with free access to standard laboratory food and water, were killed by decapitation. Tissues were rapidly removed, mounted on microtome chucks, frozen in dry ice, and stored at −80°C. Human brain and spinal cord were obtained at autopsy (postmortem delay, 6 ± 3 hr) from the Institute of Pathology, Kantonsspital, Basel, by kind permission of Professor J. Ulrich. The individuals (four males, one female), averaging 74.6 years of age, died without clinical or histopathological evidence of neurological disease. For saturation experiments, we used brain tissue from a 47 year old male 7 hr postmortem. Cryostat sections (12 μm) of all tissues were cut and mounted on precleaned slides and then stored at −20°C for up to 2 months until used.

Radioligands and enzyme inhibitors. ^{3}H-Ro 41-1049 and ^{3}H-Ro 19-6327 (specific activities 19.9 and 19.1 Ci/mmol, respectively) were synthesized by Dr. H. Harder (Isotope Synthesis Department, Hoffmann–La Roche, Basel) as previously described (Cesura et al., 1989, 1990) (Fig. 1).

The sites of tritium incorporation (in the ring part of the molecule) were chosen to avoid metabolic separation of the radiolabel by deamination. The initial purities of the two radioligands were 98% and 92%, respectively, for ^{3}H-Ro 41-1049 and ^{3}H-Ro 19-6327; these were checked at regular intervals by HPLC. Stored at −80°C, radiolytic degradation was approximately 8% per annum. A purity of ≥80% was used for all experiments.

All Roche (Ro) compounds were synthesized in the Pharma Division of Hoffmann-La Roche in Basel. Clorgyline HCl and L-deprenyl were obtained from Research Biochemicals Inc. (Natick, MA). All other chemicals were of analytical grade and obtained from various sources.

Binding conditions. The optimal conditions for radiolabeling MAO-A and MAO-B with ^{3}H-Ro 41-1049 and ^{3}H-Ro 19-6327 were obtained by determining the appropriate binding characteristics of these radioligands to tissue sections according to previously described procedures (reviewed by Kuhar and Unnerstall, 1990).

Association and dissociation kinetics, optimal rinsing, and equilibrium saturation of their binding to tissues were determined by exposing sections of rat brain to various incubation times (10 min to 4 hr), incubation temperatures (4–37°C), rinse times (5 min to 8 hr), rinse procedures (from a quick dip to 5 min + 5 min + 10 min), and ligand concentrations (1–250 nM).

A buffer solution (pH 7.4) containing 50 mM Tris, 120 mM NaCl, 1 mM $MgCl_2$, 5 mM KCl, and 0.5 mM EGTA was used in all experiments. Nonspecific binding was determined by incubating adjacent sections under identical conditions with 1 μM clorgyline or L-deprenyl (for ^{3}H-Ro 41-1049 and ^{3}H-Ro 19-6327 binding, respectively); to determine the nonspecific binding in saturation experiments, we used 50 μM clorgyline or L-deprenyl. Competition binding experiments were carried out with the following compounds at 1 μM: Ro 41-1049, Ro 40-8841, Ro 41-3549, Ro 19-6327, Ro 18-9374, and Ro 18-7420 (see Fig. 3 for chemical structures). IC_{50} values for Ro 19-6327, Ro 41-1049, clorgyline, and L-deprenyl were estimated from competition binding inhibition curves in both binding assays using concentrations ranging between 1 nM and 1 mM according to the potency of each compound.

Quantitation of binding to sections. Radioactivity was determined first by wiping the wet tissues from the slides with Whatman GF/B glass microfiber disks, which were then soaked in 2 ml Soluene overnight with agitation before liquid scintillation counting 24 hr later (the recovery of this method was consistent since the values of five replicate measurements varied by <5%). Tissue sections, together with brain paste standards and plastic standards (tritium scales, Amersham), were then exposed to tritium-sensitive LKB Ultrofilm for 3 weeks before development in Kodak D-19 (5 min at 20°C). After calibration of the film (with corrected tritium scales), densitometric analyses of radioautograms were performed using a computer-assisted image analysis system (ASBA, Wild-Leitz, Zürich). Optical densities were converted into pmol/mg protein.

The films were used as negatives to produce reverse images, that is, white areas revealing high binding densities on a black background. Neuroanatomical regions were identified with the aid of a stereotaxic rat brain atlas (Paxinos and Watson, 1986) and atlases of the human brain (Nieuwenhuys et al., 1988; De Armond et al., 1989; Paxinos, 1990).

Whereas association and dissociation binding data were analyzed by KINETIC (McPherson, 1985), saturation and competition binding data were determined by the nonlinear curve-fitting program LIGAND (McPherson, 1985).

MAO-A and MAO-B activity in tissue homogenates was determined radiochemically according to Wurtman and Axelrod with some modifications (Da Prada et al., 1989a).

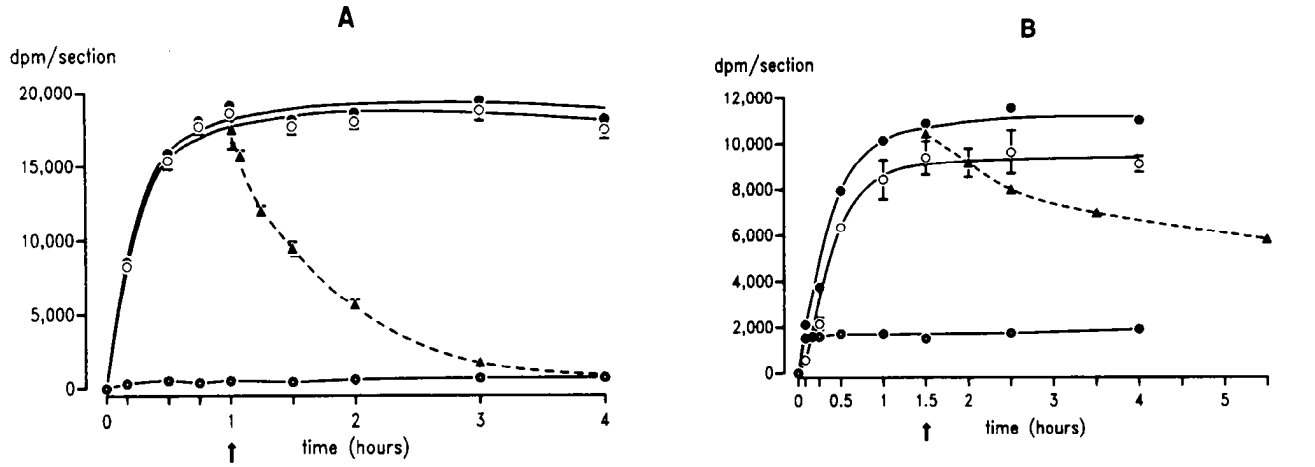

Figure 2. In vitro binding kinetics in parasagittal sections of rat brain of ^{3}H-Ro 41-1049 (15 nM; *A*) and ^{3}H-Ro 19-6327 (20 nM; *B*) at 37°C and 20°C, respectively. Values are from two experiments (four replicates each). *Error bars* show SEM (for the association and dissociation of specific binding only). Note the rapid association of both radioligands and their slow dissociation (▲) induced by 1 μM of the respective nonradioactive compounds at the respective times (*arrows*). ●, total binding; ○, specific binding; ⊙, nonspecific binding (in the presence of 1 μM clorgyline and L-deprenyl, respectively).

Results

Tissue preparation

In the present studies we used fresh-frozen tissues since mild or strong perfusion fixation (with 0.1% paraformaldehyde or 2% paraformaldehyde plus 1% glutaraldehyde, respectively) reduced total binding by 10–13% or even by a greater extent with concomitant lower specific-to-nonspecific binding ratios (see also Yoo et al., 1974). After cryosectioning, the tissues could be stored for at least 2 months at −17°C without significant loss of either radioligand bindings, whereas storage at 4°C virtually halved the binding capacity.

Binding characteristics

Association and dissociation kinetics. The kinetics and equilibrium binding of ^{3}H-Ro 41-1049 and ^{3}H-Ro 19-6327 were determined in slide-mounted tissue sections (wipe-off method and scintillation counting). Specific binding of the two radioligands increased with the incubation time. Steady state was reached after 60 min incubation at 37°C for ^{3}H-Ro 41-1049 and after 90 min incubation at 20°C for ^{3}H-Ro 19-6327 (Fig. 2). These conditions were used for subsequent equilibrium-binding experiments.

The dissociation half-times ($t_{1/2}$), determined by immersing tissue sections in buffer medium containing 15 nM ^{3}H-Ro 41-1049 or 20 nM ^{3}H-Ro 19-6327 until equilibrium was reached and then subjecting them to various incubation times in buffer (in the presence of 1 μM nonradioactive compound to avoid "rebinding"), were 30 min and 8 hr, respectively (Fig. 2). The rinse time, which provided the highest specific-to-nonspecific binding ratios without significant loss in specific binding, was determined to be 30 sec + 30 sec + 60 sec in ice-cold buffer followed by a quick rinse in ice-cold distilled water. Nonspecific binding under these rinse conditions was ≤5% or ≤10%, respectively, for ^{3}H-Ro 41-1049 and ^{3}H-Ro 19-6327.

Pharmacological specificity. The pharmacological specificities of the respective binding assays were determined with various MAO inhibitors by competition analysis, with inactive compounds serving as controls (Fig. 3). The degree of binding inhibition and enzyme inhibition correlated highly for the respective enzymes in various tissues; that is, only active MAO-A and MAO-B inhibitors competed for ^{3}H-Ro 41-1049 and ^{3}H-Ro 19-6327 binding, respectively.

IC_{50} values for MAO inhibitors. Competition for ^{3}H-Ro 41-1049 and ^{3}H-Ro 19-6327 binding to rat brain sections by known selective MAO-A or MAO-B inhibitors produced inhibition curves (Fig. 4) and IC_{50} values whose rank order corresponded very well with their potencies as enzyme inhibitors (Table 1).

Saturation experiments. The steady state binding of the respective radioligands to rat brain sections was of a high affinity and saturable (Fig. 5). Nonspecific binding (determined in the presence of 50 μM clorgyline or L-deprenyl) was linear over the range of radioligand concentrations used and was 3–7% of the total binding at K_D. Analysis of the saturation data revealed apparent K_D values for ^{3}H-Ro 41-1049 and ^{3}H-Ro 19-6327 of 13.7 ± 1.2 nM and 19.3 ± 1.8 nM, respectively (averages of 22 rat brain regions). The K_D values obtained for different regions of human brain are shown in Table 2. They reveal a four- to fivefold regional difference for each inhibitor; similar differences were found for rat brain regions (results not shown).

Distribution and abundance of binding sites in rat tissues

Quantitative enzyme radioautography and image analysis revealed high-affinity, saturable, and pharmacologically specific binding of ^{3}H-Ro 41-1949 and ^{3}H-Ro 19-6327 (at steady state and K_D concentrations) in various regions of rat CNS, peripheral organs, and postmortem human brain (Tables 2–4, Figs. 6–15). Numerous rat tissues possessed a much higher binding capacity for ^{3}H-Ro 41-1049 than for ^{3}H-Ro 19-6327. Whereas the ratio of MAO-A to MAO-B was, on average, 2 in rat brain, in other tissues much higher values were obtained, for example, 458 in the atrioventricular valve, 129 in the inner ventricular wall of the heart, 33.5 in the anterior lobe of the pituitary, 88.7 in the exocrine pancreas, and 5–6.5 in the choroid plexus, A5 cells, deep mesencephalic nuclei, and the ganglion cell and inner plexiform layers of the retina. On the other hand, the lowest MAO-A:MAO-B ratios were obtained in the inner region of the olfactory nerve layer in the bulb (0.2), in the pineal gland (0.2), subfornical organ (0.2), and posterior lobe of the pituitary (0.4).

The relative abundance of binding sites for the two radioli-

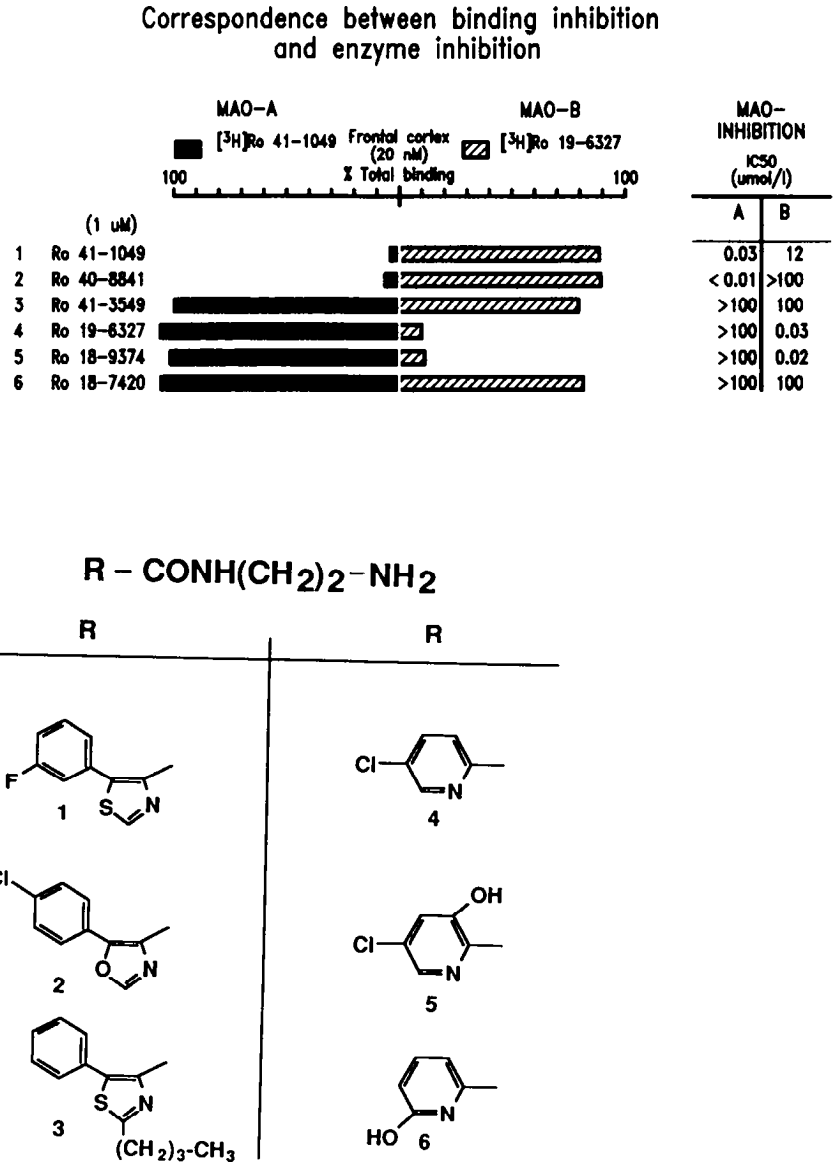

Figure 3. Correspondence between binding inhibition (histograms) and enzyme inhibition (mean IC_{50} values). Note that only the potent enzyme inhibitors (compounds *1* and *2* for MAO-A and compounds *4* and *5* for MAO-B) are able to inhibit competitively (at 1 μM) the respective binding of the radioligands. The corresponding inactive compounds (*3* and *6*) are unable to compete in the binding assays.

gands varied among the rat CNS regions and peripheral organs investigated (Tables 3, 4; Figs. 6–11). ^{3}H-Ro 41-1049 binding was highest (>6.9 pmol/mg protein) in medial habenular nucleus, locus coeruleus, ventromedial hypothalamic nucleus, and solitary tract nucleus. In contrast, equally high amounts of ^{3}H-Ro 19-6327 binding were found in virtually all circumventricular organs (organum vasculosum lamina terminalis, subfornical organ, arcuate nucleus, median eminence, pineal gland, subcommissural organ, area postrema, other ventricular ependyma), inner region of the olfactory bulb nerve layer, paraventricular thalamus, mammillary nuclei, raphe nuclei, posterior lobe of the pituitary, lateral part of the interpeduncular nucleus, and periventricular hypothalamus.

In the peripheral tissues investigated (Table 4; Figs. 10, 11), a high abundance of binding sites for ^{3}H-Ro 41-1049 was observed in both exocrine and endocrine pancreas, vas deferens, liver, superior cervical ganglion, duodenum, and heart, whereas ^{3}H-Ro 19-6327 binding was highest in the endocrine pancreas, epididymis, liver (periportal > central regions), and duodenum. Of all the rat tissues so far investigated, brain white matter and skeletal muscle contained the least number of binding sites for either radioligand. Furthermore, little or no binding of ^{3}H-Ro 19-6327 in heart and exocrine pancreas was observed.

The highest abundance of binding sites for either enzyme in the rat brain was found in the locus coeruleus (^{3}H-Ro 41-1049 binding) and the lowest in white matter. Of the peripheral organs investigated, superior cervical ganglion (MAO-A) and liver (MAO-B) contained the highest abundance of enzyme binding sites, whereas skeletal muscle (MAO-A and MAO-B) contained the lowest.

The binding capacities of the peripheral organs and brain regions for ^{3}H-Ro 41-1049 and ^{3}H-Ro 19-6327 correlated extremely well with the respective enzyme activities of the tissues (Fig. 12).

Resolution of the technique

Despite the inherent resolution limits of radioautography, it was possible to reveal the discrete distribution—in a few instances the cellular location—of enzyme binding sites in certain brain regions and peripheral organs of the rat (Figs. 9, 13, 14). By

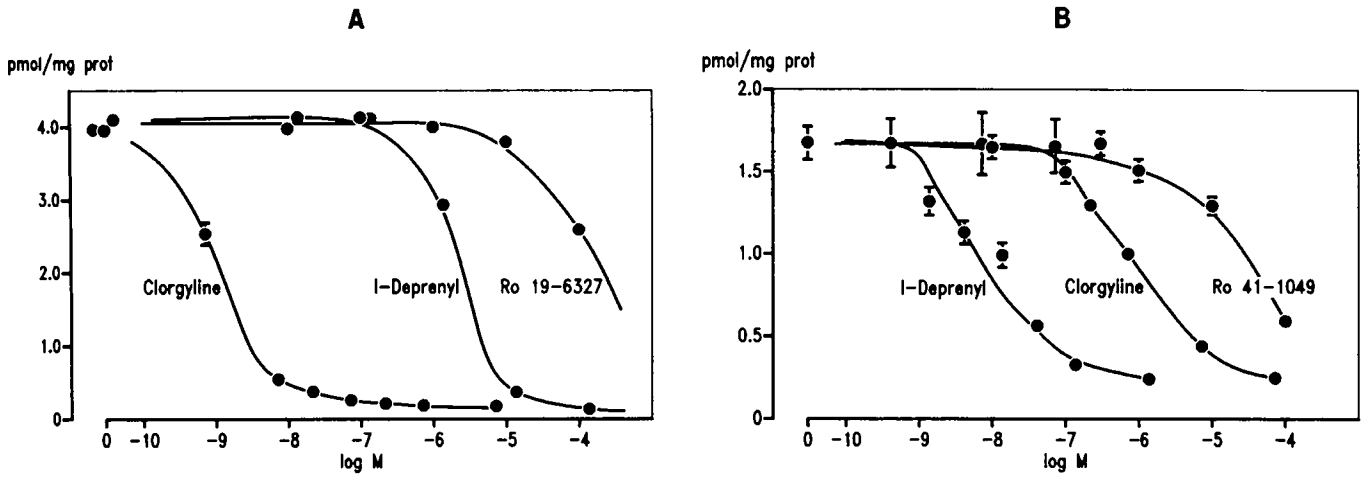

Figure 4. Competitive inhibition by MAO inhibitors of ^{3}H-Ro 41-1049 binding (*A*) and ^{3}H-Ro 19-6327 binding (*B*) (20 nM) to rat frontal cortex *in vitro*. Data are from a single experiment (three replicates). *Error bars* show SEM (for most points they are too small to be visible). Note the potencies of the MAO-A inhibitor clorgyline and the MAO-B inhibitor L-deprenyl in *A* and *B*, respectively, as well as the relative selectivities of Ro 19-6327 versus L-deprenyl and Ro 41-1049 versus clorgyline.

apposing emulsion-coated coverslips to the radiolabeled tissue sections for various times, accumulations of silver grains could be observed (by dark-field or bright-field microscopy) overlaying histologically defined cells. ^{3}H-Ro 19-6327, for example, was found to bind to ventricular ependymal cells (including those of circumventricular organs) in the brain and to pancreatic islet cells and, as yet unidentified, renal tubuli. ^{3}H-Ro 41-1049, on the other hand, bound to noradrenergic neurons in superior cervical ganglion, to A4, A5, A6, A7, C1, and C3 cells, and to the ganglion cell layer in the retina.

Distribution and abundance of binding sites in human brain

In radiolabeled sections of human postmortem brain (Figs. 15, 16), binding sites for ^{3}H-Ro 19-6327 were generally found to be more abundant than those for ^{3}H-Ro 41-1049, that is, opposite to rat brain. A comparison of the B_{max} and K_D values for the human brain regions investigated (caudate, putamen, hippocampal formation, substantia nigra, cerebellum) revealed much lower binding capacities for ^{3}H-Ro 41-1049 than for ^{3}H-Ro 19-6327 (Table 2). Whereas MAO-A was abundant in the interpeduncular nucleus, periaqueductal gray, substantia nigra (pars compacta), and locus coeruleus, MAO-B was most concentrated in ependymal cells, polymorphic layer of the dentate gyrus, dorsal raphe nucleus, substantia nigra (pars reticulata), and interpeduncular nucleus. The lowest levels of both enzymes were found in white matter.

Discussion

Inactivation of released monoamine neurotransmitters (Trendelenburg, 1990) occurs by their selective neuronal reuptake and extraneuronal uptake via selective transporters. This inactivation is indirectly facilitated by the enzymes MAO and COMT (catechol-*O*-methyltransferase), which maintain a low cytosolic amine concentration in monoaminergic neurons and other cells (e.g., glia).

The present findings demonstrate that the distribution and abundance of MAO-A and MAO-B in discrete areas of rat CNS, peripheral organs, and human postmortem brain can be revealed by quantitative enzyme radioautography. The technique described satisfies several criteria that are considered to be important for establishing a reliable enzyme assay: binding was of a high affinity, saturable, pharmacologically selective, and tissue specific. Binding values were highly reproducible with a small margin of error. Moreover, the extremely good correlation between binding and enzyme activity indicates that the method provides a means to assay the active enzyme in tissue sections. Thus, in analogy to receptor radioautography (Kuhar and Unnerstall, 1990), this approach can be used also for quantitative enzyme mapping using radiolabeled inhibitors as high-affinity substrates (see also Chai et al., 1990). The results furthermore indicate that the two enzymes have distinct anatomical distributions, which confirms and extends findings of previous en-

Table 1. Correspondence between IC_{50} values for MAO-A and MAO-B activity and ^{3}H-Ro 41-1049 and ^{3}H-Ro 19-6327 binding *in vitro* with different MAO inhibitors

	Enzyme inhibition		Binding inhibition	
Inhibitor	MAO-A activity	MAO-B activity	^{3}H-Ro 41-1049	^{3}H-Ro 19-6327
Clorgyline	1.0 (0.7–1.3) nM	0.7 (0.6–0.8) μM	1.0 (0.8–1.2) nM	0.8 (0.4–1.8) μM
L-Deprenyl	1.4 (0.7–3.1) μM	5.8 (3.4–9.9) nM	2.3 (2.2–2.6) μM	11.0 (3.4–) nM
Ro 19-6327	983 (727–1330) μM	–	185 (65–526) μM	–
Ro 41-1049	–	12.0 (11.5–12.7) μM	–	38.0 (20.2–71.7) μM

Shown are calculated IC_{50} values and, in parentheses, 95% confidence limits. Binding data were derived from the data shown in Figure 4.

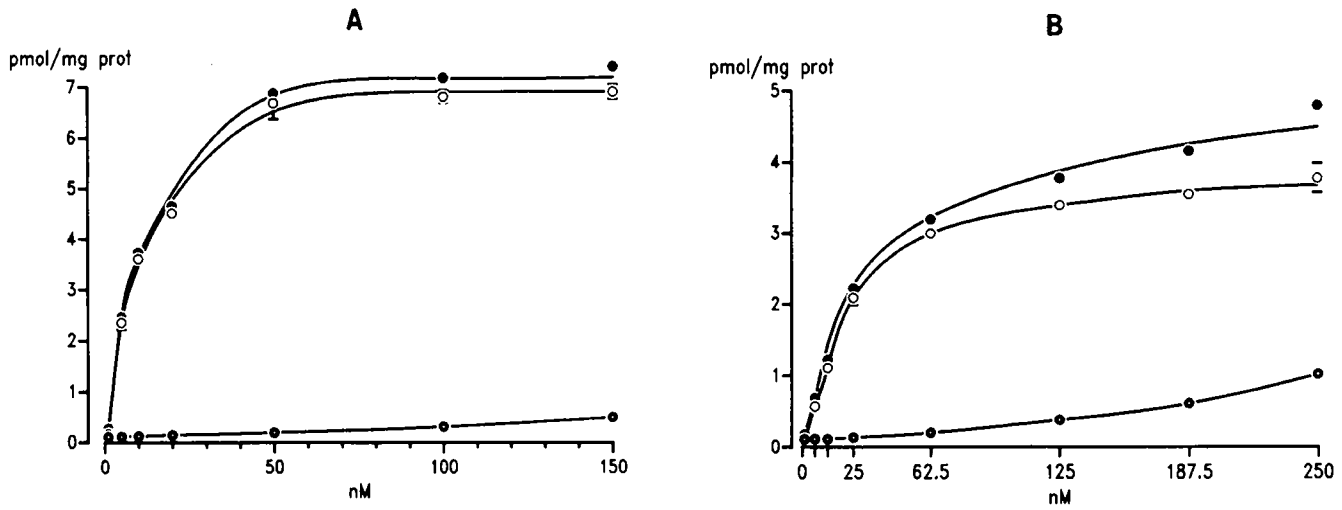

Figure 5. Saturation of ^{3}H-Ro 41-1049 binding (*A*) and ^{3}H-Ro 19-6327 binding (*B*) to sections of rat brain frontal cortex *in vitro* under steady state conditions. Data are from two experiments (three replicates). *Error bars* (where visible) show SEM (only for specific binding). ●, total binding; ○, specific binding; ◘, nonspecific binding. Half-saturation of specific binding occurred at 10.7 nM for ^{3}H-Ro 41-1049 and 18.4 nM for ^{3}H-Ro 19-6327.

zyme histochemical and immunohistochemical studies. The functional significance of their respective distributions is discussed particularly in the context of the assumed preferred affinities of MAO-A and MAO-B enzymes for natural substrates and of their cellular localization.

Quantitative enzyme radioautography: binding kinetics

The radiolabeled reversible inhibitors of MAO-A and MAO-B used in the present study (^{3}H-Ro 41-1049 and ^{3}H-Ro 19-6327, respectively) are high-affinity enzyme substrates. At steady state, the specific binding of both radioligands was saturable and pharmacologically highly selective, observations that confirm and extend those obtained from analysis of binding to rat and human brain homogenates (Cesura et al., 1989, 1990).

Thus, the binding to sections of human brain was concentration and time dependent, half-saturation occurring on average with 27.6 nM for ^{3}H-Ro 41-1049 and 10.2 nM for ^{3}H-Ro 19-6327 at equilibrium, which was reached by 60 min at 37°C and 90 min at 20°C, respectively, for the MAO-A and MAO-B inhibitors. Comparable K_D values for homogenates have been reported, that is, 16.5 nM for ^{3}H-Ro 41-1049 (Cesura et al., 1990) and 5.6 nM for ^{3}H-Ro 19-6327 (Da Prada et al., 1990b).

The amounts of MAO-A and MAO-B, determined (in saturation experiments) by the capacity of tissues to bind ^{3}H-Ro 41-1049 and ^{3}H-Ro 19-6327, respectively, were of the same order of magnitude as the values derived by titration of MAO-A and MAO-B with clorgyline and L-deprenyl (Fowler et al., 1980) and by binding to homogenates (Cesura et al., 1989, 1990) and tissue sections (Reznikoff et al., 1985).

Table 2. Specific binding of ^{3}H-Ro 41-1049 and ^{3}H-Ro 19-6327 to sections of human brain *in vitro*: saturation experiments

	MAO-A				MAO-B				Ratio
Structure	K_D	±SEM	B_{max}	±SEM	K_D	±SEM	B_{max}	±SEM	B:A
Caudate nucleus	25.5	2.3	3.38	0.26	10.5	0.6	10.75	0.38	3.18
Putamen	20.8	1.7	3.43	0.16	9.9	0.4	10.16	0.27	2.96
Ependyma lateral ventricle	10.6	2.0	3.74	0.16	23.3	1.9	31.51	1.40	8.43
Entorhinal cortex	44.1	5.2	4.50	0.18	10.9	0.9	8.24	0.35	1.83
Subiculum	23.7	3.2	4.37	0.16	11.3	2.8	5.29	0.43	1.21
Pyramidal layer, CA1	24.7	3.1	4.51	0.15	8.7	1.4	3.37	0.18	0.75
Pyramidal layer, CA3	43.4	6.4	4.45	0.21	7.6	1.5	7.94	0.44	1.78
Granular layer, DG	53.8	8.8	4.30	0.24	10.9	0.5	10.43	0.31	2.43
Polymorphic layer, DG	25.2	3.4	4.46	0.16	7.5	0.2	15.00	0.21	3.36
Periaqueductal gray	19.6	3.4	6.92	0.31	8.3	0.5	8.84	0.42	1.28
Reticular formation of mesencephalon	22.3	2.7	4.53	0.15	11.3	1.0	8.79	0.23	1.94
Interpeduncular nucleus	10.3	0.9	8.80	0.16	7.9	0.6	11.09	0.78	1.26
Substantia nigra, pars compacta	14.8	1.9	5.69	0.18	10.7	1.6	12.98	0.59	2.28
Pontine nuclei	17.4	2.6	4.17	0.16	5.1	1.2	8.43	1.08	2.02
Granular layer of cerebellum	57.5	10.5	3.02	0.19	9.0	1.1	3.30	0.22	1.09

K_D values are in nM; B_{max} values are in pmol/mg protein. Data are from two experiments (three sections each per parameter) and one individual.

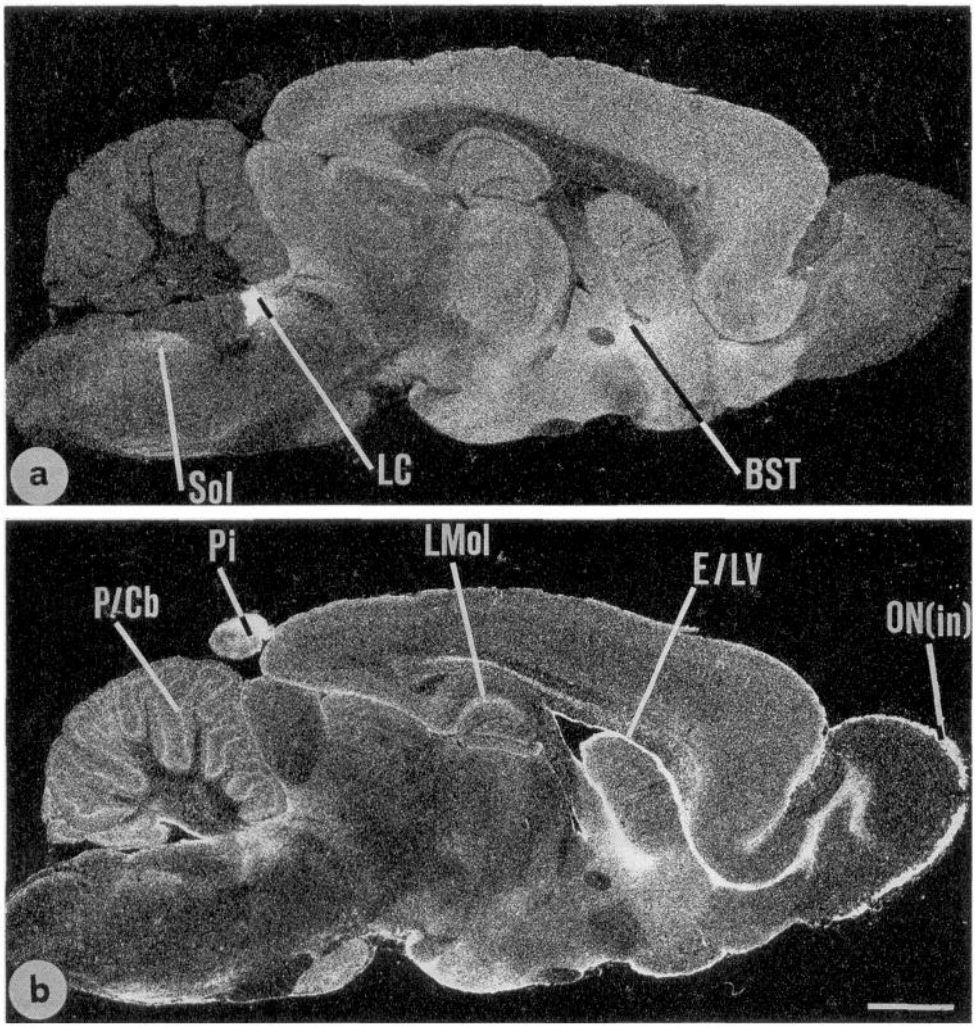

Figure 6. Distribution of the *in vitro* binding sites for ^{3}H-Ro 41-1049 (MAO-A; *a*) and ^{3}H-Ro 19-6327 (MAO-B; *b*) in adjacent parasagittal sections of rat brain under steady state conditions and at [K_D]; macroscopic images, with white areas revealing high binding density. Note the abundance of MAO-A inter alia in the bed nucleus of the stria terminalis (*BST*), locus coeruleus (*LC*), and solitary tract nucleus (*Sol*) and of MAO-B in the ependyma of the lateral ventricle (*E/LV*), lacunosum moleculare of the hippocampus (*LMol*), inner olfactory nerve layer of the bulb [*ON(in)*], Bergmann glia cells in the cerebellar Purkinje cell layer (*P/Cb*), and pineal (*Pi*). Scale bar, 2 mm.

Quantitative enzyme radioautography: distribution and abundance of MAO-A and MAO-B in rat tissues

In general, the rank order of binding values (at K_D) for the radioligands of the respective enzymes in discrete regions of the rat CNS, peripheral organs, and human postmortem brain correlated very well with the cellular distribution of enzyme activities revealed by an improved histochemical method (Arai et al., 1986; Konradi et al., 1989). Similar results, moreover, were obtained immunohistochemically using monoclonal antibodies with human peripheral tissues and brain (Westlund et al.,' 1985, 1988; Thorpe et al., 1987; Konradi et al., 1988) as well as with rat brain (Levitt et al., 1982). Although the cellular resolution of enzyme radioautography does not compare with that of enzyme histochemistry and immunohistochemistry, it is a quantitative and highly sensitive technique.

MAO-A. In rat brain, the regional distribution and abundance of ^{3}H-Ro 41-1049 binding sites were in accordance with regional MAO-A activity (Glover and Sandler, 1987), with the locus coeruleus, median habenular, and interpeduncular nuclei containing the highest levels and white matter and pineal gland the lowest. Among the peripheral organs investigated, the superior cervical ganglion and skeletal muscle contained the highest and lowest abundance of MAO, respectively, again confirming reports in the literature (Youdim et al., 1988).

MAO-B. The distribution and abundance of ^{3}H-Ro 19-6327 binding sites in rat brain differed markedly from those of ^{3}H-Ro 41-1049 but correlated with the regional localization of MAO-B (Levitt et al., 1982), with the circumventricular organs, mammillary nuclei, and posterior pituitary having the highest and white matter and anterior pituitary the lowest abundances. In the periphery, liver and skeletal muscle contained the highest and lowest amounts of the enzyme, respectively (Pintar et al., 1983; Youdim et al., 1988).

Distribution and abundance of MAO-A and MAO-B in human brainstem nuclei

Human brain regions on average contained more MAO-B than MAO-A. In cell bodies of the locus coeruleus, the high density of binding sites for ^{3}H-Ro 41-1049 indicates an abundance of MAO-A. Although the resolution of the method does not allow us to exclude a moderate level of ^{3}H-Ro 19-6327 binding to these cells (i.e., the presence of MAO-B), recent observations from *in situ* hybridization histochemistry suggest that locus coeruleus cells contain mRNA encoding for MAO-A but not for MAO-B (Richards et al., 1992).

On the other hand, cell bodies of the raphe nuclei (in the same plane of section) contained a high density of binding sites for ^{3}H-Ro 19-6327 but not for ^{3}H-Ro 41-1049; that is, they contain

Table 3. Specific binding of ^{3}H-Ro 41-1049 and ^{3}H-Ro 19-6327 (pmol/mg protein) to rat CNS *in vitro* (at [K_D])

Structure	MAO-A		MAO-B		A:B
	Mean	SEM	Mean	SEM	
Cortex					
Frontal cortex					
Layer 1	3.83	0.02	3.45	0.07	1.1
Layer 2, 3	3.76	0.01	1.81	0.09	2.0
Layer 4–6	3.79	0.01	1.61	0.05	2.4
Claustrum	5.94	0.29	2.28	0.07	2.6
Piriform cortex	3.69	0.02	1.24	0.05	3.0
Cingulate cortex	3.92	0.04	2.87	0.10	1.4
Olfactory bulb					
Internal granular layer	3.43	0.04	0.79	0.02	4.4
Mitral and plexiform	2.13	0.02	0.80	0.04	2.7
Glomerular layer	2.11	0.09	1.64	0.07	1.3
Olfactory nerve layer					
Inner part	1.35	0.09	7.49	0.12	0.2
Outer part	1.36	0.07	0.67	0.07	2.0
Telencephalon					
Hippocampus and septum					
Fimbria	2.00	0.05	1.53	0.04	1.3
Bed nucleus of stria terminalis	6.88	0.20	3.42	0.08	2.0
CA1 hippocampus					
Oriens	3.91	0.02	3.37	0.04	1.2
Pyramidal	3.47	0.02	3.10	0.06	1.1
Stratum radiatum	3.97	0.03	2.58	0.07	1.5
Lacunosum moleculare	4.05	0.04	3.96	0.04	1.0
Dentate gyrus					
Molecular	4.05	0.04	3.34	0.04	1.2
Granular	3.54	0.02	3.31	0.05	1.1
Basal ganglia					
Caudate putamen	3.79	0.02	1.83	0.04	2.1
Globus pallidus	2.83	0.08	1.07	0.04	2.7
Nucleus of lateral olfactory tract	6.79	0.08	1.56	0.06	4.4
Internal capsule	1.12	0.05	0.39	0.01	2.9
Remaining telencephalic areas					
Nucleus accumbens	6.05	0.36	3.81	0.20	1.6
Cingulum	3.07	0.10	5.79	0.39	0.5
Corpus callosum	2.38	0.09	1.91	0.07	1.2
Diencephalon					
Epithalamus					
Stria medullaris thalami	2.36	0.18	1.17	0.11	2.0
Medial habenular nucleus	8.04	0.27	4.90	0.08	1.6
Thalamus					
Paraventricular	7.37	0.03	6.90	0.07	1.1
Laterodorsal	5.07	0.14	2.65	0.04	1.9
Ventrolateral	3.78	0.04	1.57	0.07	2.4
Medial geniculate	4.95	0.14	2.55	0.12	1.9
Hypothalamus					
Periventricular hypothalamus	5.62	0.11	7.81	0.13	0.7
Ventromedial hypothalamic nucleus	7.00	0.08	4.11	0.06	1.7
Supraoptic nucleus	4.39	0.20	5.26	0.10	0.8
Lateral mammillary nucleus	4.56	0.12	5.82	0.19	0.8
Tuberomammillary nucleus	5.03	0.07	6.67	0.16	0.8
Mesencephalon					
Tectum					
Superior colliculus					
Superficial gray	4.48	0.11	3.28	0.04	1.4
Intermediate gray	3.73	0.02	3.16	0.07	1.2
Inferior colliculus					
Central nucleus	3.58	0.04	1.80	0.03	2.0

Table 3. Continued

Structure	MAO-A Mean	MAO-A SEM	MAO-B Mean	MAO-B SEM	A:B
Tegmentum					
Interpeduncular nucleus					
Lateral	9.17	0.36	6.92	0.03	1.3
Caudal/intermediate	7.63	0.01	3.61	0.05	2.1
Substantia nigra					
Pars reticulata	3.41	0.05	1.19	0.08	2.9
Pars compacta	3.95	0.03	1.20	0.06	3.3
Ventral tegmental area	4.03	0.08	2.43	0.07	1.7
Central gray	5.25	0.16	3.65	0.03	1.4
Deep mesencephalic nucleus	2.48	0.07	0.47	0.01	5.2
Rhombencephalon					
Cranial nerves nucleus					
Nucleus of solitary tract	7.10	0.04	4.15	0.06	1.7
Hypoglossal nucleus	3.97	0.02	2.25	0.08	1.8
Raphe nuclei					
Median	4.49	0.15	7.08	0.07	0.6
Dorsal	5.91	0.20	7.80	0.03	0.8
Remaining rhombencephalic nuclei					
Pontine nuclei	3.05	0.07	3.46	0.06	0.9
Locus coeruleus	16.54	1.46	4.11	0.08	4.0
Inferior olives	4.21	0.09	4.11	0.09	1.0
A5 cells	3.97	0.04	0.75	0.07	5.3
C1 cells	4.87	0.21	1.23	0.11	4.0
Rhombencephalic fiber system					
Facial nerve	0.31	0.04	0.22	0.03	1.4
Cerebellum					
Molecular layer	3.07	0.10	2.36	0.08	1.3
Granular layer	3.23	0.06	2.39	0.04	1.3
Purkinje cells layer	3.10	0.03	3.42	0.02	0.9
White matter	0.50	0.01	0.34	0.02	1.4
Spinal cord					
Layers 1–3	3.14	0.08	2.66	0.15	1.2
Layers 7–9	1.85	0.02	0.55	0.01	3.4
Layer 10 (central canal)	3.08	0.07	3.63	0.07	0.8
Ventral funiculus	0.11	0.01	0.15	0.01	0.7
Circumventricular organs					
Vascular organ Lamina terminalis	4.02	0.13	14.40	2.24	0.3
Subfornical organ	3.70	0.02	16.29	4.25	0.2
Subcommisural organ	2.83	0.55	8.66	1.03	0.3
Ependyma					
Lateral ventricle	4.15	0.19	7.96	0.03	0.5
Choroid plexus					
Lateral ventricle	3.07	0.22	0.55	0.03	5.6
Arcuate nucleus	4.73	0.15	9.51	0.59	0.5
Median eminence	3.75	0.03	7.04	0.11	0.5
Pineal gland	1.75	0.13	10.51	2.84	0.2
Area postrema	3.82	0.04	7.35	0.02	0.5
Pituitary					
Posterior lobe	2.93	0.14	7.29	0.10	0.4
Intermediate lobe	3.43	0.10	0.67	0.09	5.1
Anterior lobe	3.72	0.05	0.11	0.01	33.5
Retina					
Ganglion cell–inner plexiform layers	2.02	0.30	0.31	0.03	6.5
Remaining layers	0.20	0.04	0.04	0.01	5.3

Values are means of five animals (per brain; 15–26 levels, six sections per level: four total binding, two nonspecific binding). The ratios of half-maximal binding to MAO-A versus MAO-B are shown in the right column.

Table 4. Specific binding of ^{3}H-Ro 41-1049 and ^{3}H-Ro 19-6327 (pmol/mg protein) to sections of rat peripheral organs *in vitro* (at [K_D])

	MAO-A		MAO-B		
Structure	Mean	SEM	Mean	SEM	A:B
Spleen					
Red pulp	1.05	0.04	0.17	0.01	6.3
White pulp	0.37	0.02	0.04	0.01	9.2
Pancreas					
Exocrine pancreas	4.24	0.03	0.05	0.01	88.7
Islets of Langerhans	4.02	0.12	5.15	0.12	0.8
Kidney					
Renal cortex					
Tubuli	2.43	0.05	1.98	0.08	1.2
Remaining cortex	2.43	0.05	0.10	0.01	24.6
Outer medulla					
Outer zone	1.26	0.03	0.09	0.01	14.0
Inner zone	1.83	0.04	0.09	0.01	20.8
Inner medulla	1.32	0.04	0.08	0.01	17.3
Ureter	4.06	0.54	1.87	0.08	2.2
Adrenal gland					
Cortex	3.59	0.13	0.29	0.01	12.3
Medulla	2.48	0.22	0.40	0.01	6.1
Vas deferens	3.01	0.02	0.23	0.01	13.1
Epididymis	2.65	0.04	4.38	0.21	0.6
Liver					
Periportal regions	7.49	0.01	15.96	2.62	0.5
Central regions	7.33	0.03	10.30	0.79	0.7
Superior cervical ganglion	12.04	1.07	2.37	0.06	5.1
Muscle	0.27	0.01	ND	—	—
Lung	1.91	0.03	1.89	0.06	1.0
Duodenum					
Muscularis externa	4.08	0.09	3.54	0.05	1.2
Submucosa	3.21	0.14	0.23	0.05	14.0
Intestinal villi	5.00	0.14	2.19	0.04	2.3
Heart					
Inner ventricular wall	4.78	0.25	0.04	0.02	129.1
Outer ventricular wall	1.00	0.08	0.04	0.01	23.1
Atrioventricular valve	6.42	0.46	0.01	0.01	458.4

Values are means of three animals (six sections each: four total binding, two nonspecific binding). The ratios of half-maximal binding to MAO-A versus MAO-B are shown in the right column. ND, not detected.

MAO-B but probably not MAO-A. Furthermore, raphe cells contain mRNA coding for MAO-B but not MAO-A (Richards et al., 1992).

In the substantia nigra, both MAO-A and MAO-B are present but with clearly distinct patterns of distribution as indicated by radioligand binding. However, although the melanin-containing A9 cells appeared to contain more MAO-A than MAO-B, a hybridization signal for neither MAO-A nor MAO-B mRNA could be detected (Richards et al., 1992). Enzyme histochemical and immunohistochemical investigations have failed to demonstrate the presence of either enzyme in the majority of A9 cells (Konradi et al., 1988; Westlund et al., 1988; Moll et al., 1990). The functional implications of these findings are currently the subject of much speculation.

Is the cellular localization of the enzymes in accordance with the distribution of their assumed preferred natural substrates?

Since the preferred natural substrates of MAO-A (in rat brain *in vitro*) are assumed to be noradrenaline, dopamine, and 5-HT, and those of MAO-B, several trace amines (phenethylamine, tryptamine, methylhistamine), the cellular localization of the enzymes might be expected to reflect the distribution of the respective monoaminergic neurons and their projections on the one hand (Björklund and Lindvall, 1984; Hökfelt et al., 1984a,b; Moore and Card, 1984; Steinbusch, 1984; Steinbusch and Mulder, 1984), and of trace amines on the other (Juorio, 1988). The present findings, confirming previous reports, suggest that this assumption is only partly correct. Whereas MAO-A is contained in noradrenergic and adrenergic neurons, MAO-B occurs in serotoninergic neurons, ependyma, circumventricular organs, as well as in glia cells. Obviously, with the inherent limitation of resolution with radioautography, we cannot exclude the possibility that the enzymes are present in other cellular compartments, for example, MAO-A in dopaminergic neurons and in glia and MAO-B in histaminergic neurons.

MAO-A. A careful comparison of the distribution of MAO-A (revealed by ^{3}H-Ro 41-1049 binding) with that of tyrosine hydroxylase–immunoreactive cells and their processes in rat brain

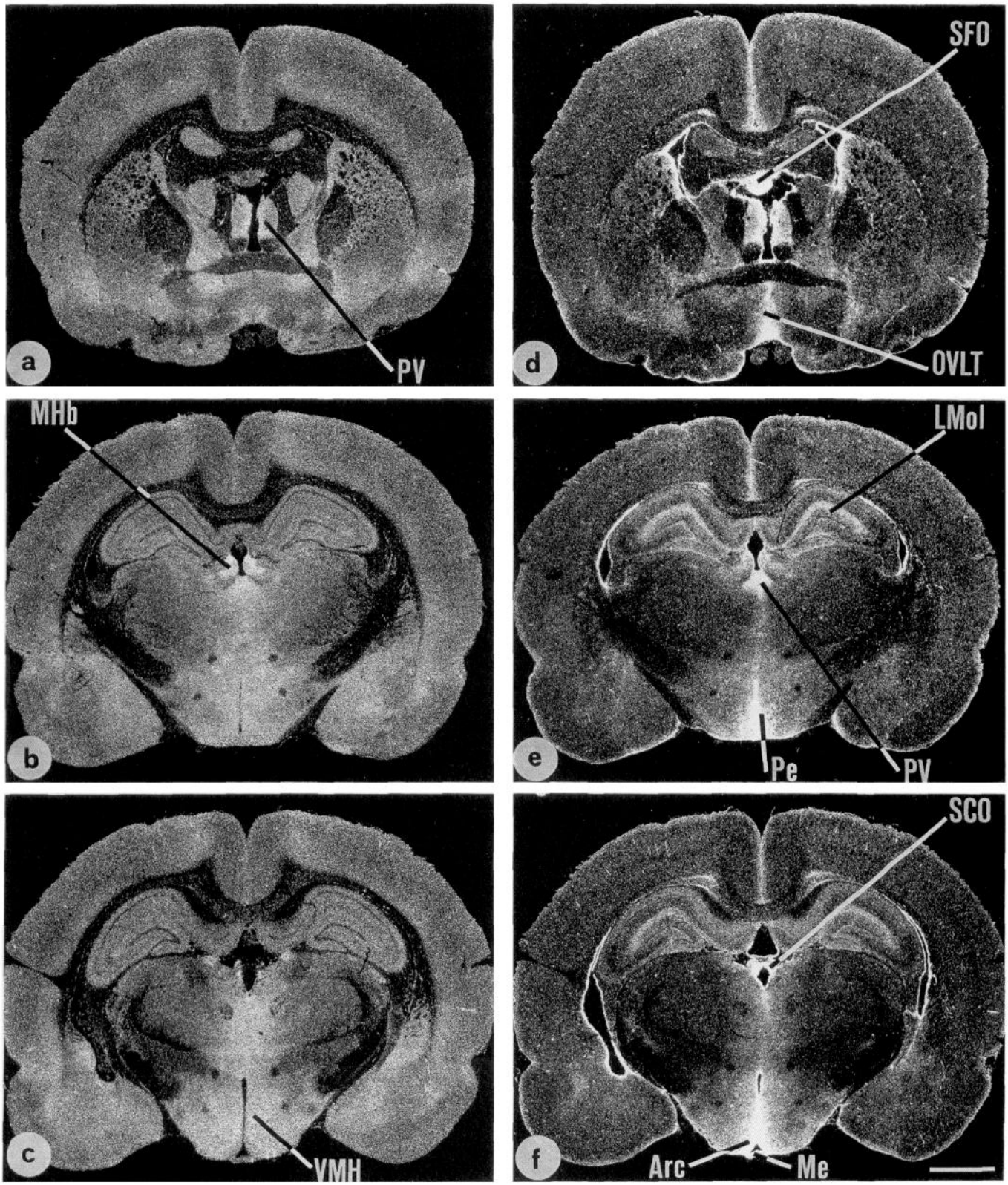

Figure 7. Distribution of the *in vitro* binding sites for ^{3}H-Ro 41-1049 (MAO-A; *a–c*) and ^{3}H-Ro 19-6327 (MAO-B; *d–f*) in adjacent frontal sections of rat brain under steady state conditions and at [K_D]; macroscopic images, with white areas revealing high binding density. Note the differences between the two enzymes in some brain regions: subfornical organ (*SFO*), organum vasculosum lamina terminalis (*OVLT*), lacunosum moleculare of the hippocampus (*LMol*), subcommissural organ (*SCO*), periventricular hypothalamus (*Pe*), ventromedial hypothalamus (*VMH*), arcuate nucleus (*Arc*), and median eminence (*Me*). In other regions the distribution is similar: paraventricular thalamus (*PV*) and median habenular nucleus (*MHb*). Scale bar, 2 mm.

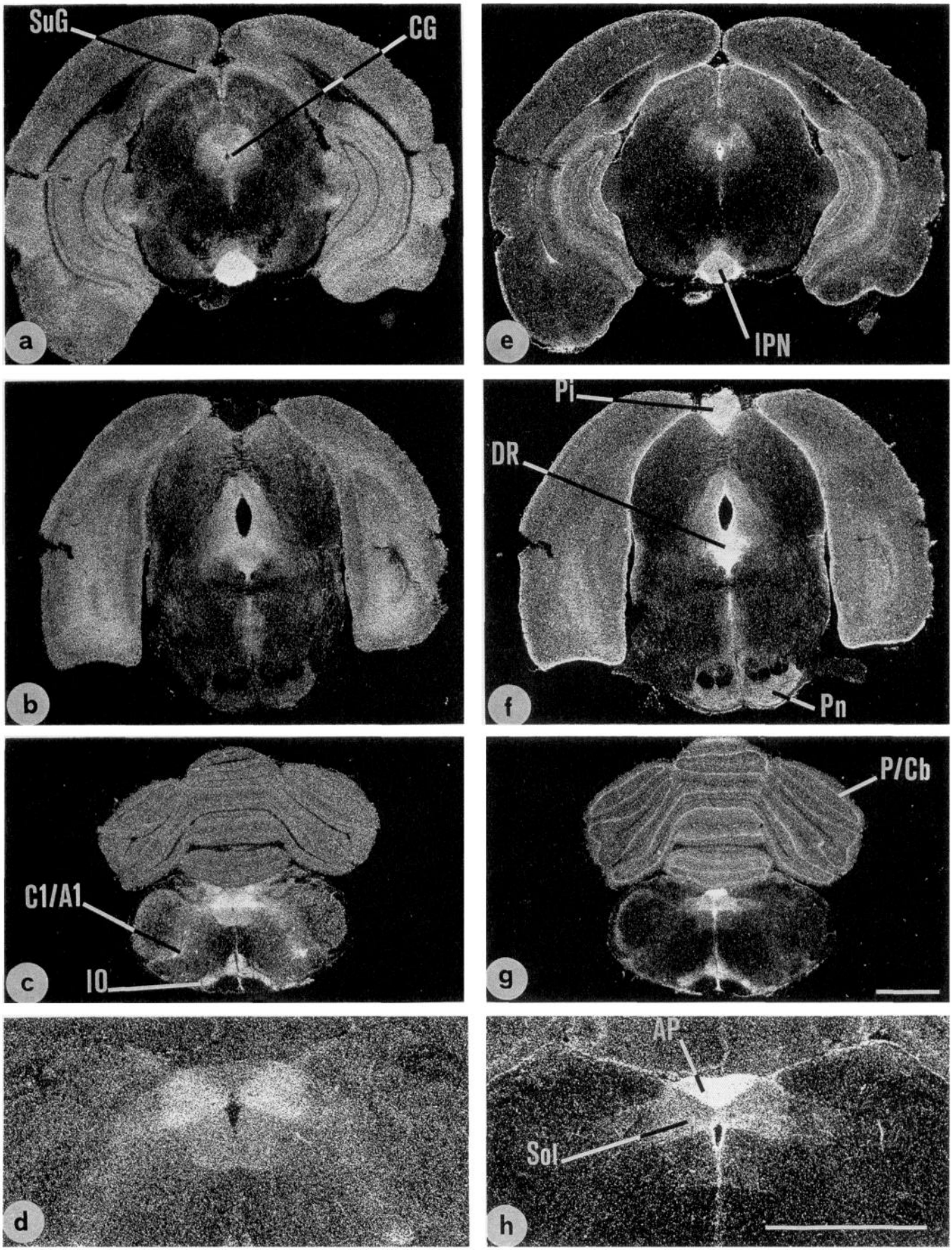
SuG
CG
a
e
IPN
b
Pi
DR
f
Pn
C1/A1
c
IO
P/Cb
g
d
AP
Sol
h

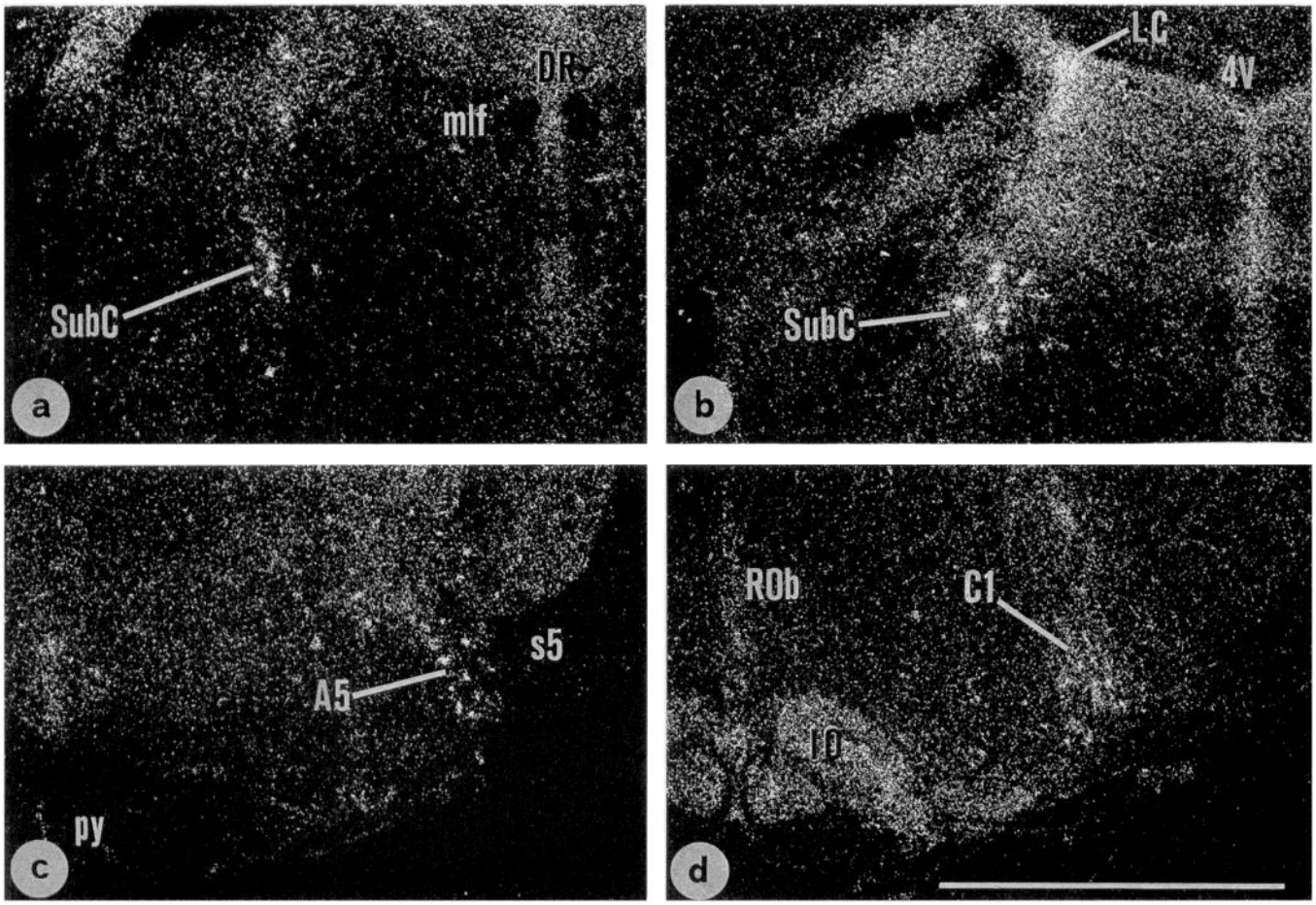

Figure 9. Macroscopic images of rat brain in frontal sections at high magnification revealing the localization of MAO-A in catecholaminergic cells. Images show distribution of the *in vitro* binding sites for ^{3}H-Ro 41-1049 (MAO-A) and ^{3}H-Ro 19-6327 (MAO-B) in adjacent sections under steady state conditions and at [K_D]; white areas reveal high binding density. Individual MAO-A–positive neurons can be seen in the nucleus subcoeruleus (*SubC*; *a, b*), *A5* cell group (*c*), and *C1* cell group (*d*). Note also the abundance of MAO-A in the locus coeruleus (*LC*; *b*), where the high density of noradrenergic neurons does not allow individual cells to be resolved. *DR,* dorsal raphe nucleus; *mlf,* medial longitudinal fasciculus; *4V,* fourth ventricle; *py,* pyramidal tract; *s5,* sensory root of the trigeminal nerve; *IO,* inferior olives; *ROb,* raphe obscurus nucleus. Scale bar, 2 mm.

(Hökfelt et al., 1984b) suggests that the enzyme is present in noradrenergic neurons (cell groups A4–7 and probably A1, A2) and in adrenergic neurons (cell groups C1, C3, and perhaps C2) (Hökfelt et al., 1984a). Although MAO-A was found in brain regions known to contain dopaminergic neurons (cell groups A8–A10 of the substantia nigra and ventral tegmental area, A12–A15 of the hypothalamus, and A6 of the olfactory bulb) (Björklund and Lindvall, 1984) and serotoninergic neurons (dorsal, median, magnus, pallidus, and obscurus raphe nuclei; Steinbusch, 1984; Riederer et al., 1990), the enzyme could not be unequivocally localized, by enzyme radioautography, to the cell bodies of these neurons (human A9 neurons being a possible exception). Most of the MAO-A–rich areas (median habenular nucleus, paraventricular thalamus, periventricular hypothalamus, solitary tract nucleus, bed nucleus of the stria terminalis) also have a rich noradrenergic innervation (Moore and Card, 1984). However, in some brain regions with a rich MAO-A content, the noradrenergic innervation is either moderate (interpeduncular nucleus) or extremely weak (ventromedial hypothalamus). In other brain regions with a heterogeneous innervation (nucleus accumbens, central gray, hippocampal formation, hypothalamus, cerebral cortex), the distribution of MAO-A was rather homogeneous, suggesting the presence of the enzyme in additional cellular compartments.

The presence of MAO-A in noradrenergic neurons of the rat and human brain and periphery is supported by the following observations: (1) enzyme histochemical and immunohistochemical as well as radioautographical evidence for the presence

←

Figure 8. Distribution of the *in vitro* binding sites for ^{3}H-Ro 41-1049 (MAO-A; *a–d*) and ^{3}H-Ro 19-6327 (MAO-B; *e–h*) in adjacent frontal sections of rat brain under steady state conditions and at [K_D]; macroscopic images, with white areas revealing high binding density. Note the differences between the two enzymes in some brain regions: superficial gray of the superior colliculus (*SuG*), pineal (*Pi*), pontine nucleus (*Pn*), adrenergic and noradrenergic cell body regions (*C1/A1*), Bergmann glia cells in the cerebellar Purkinje cell layer (*P/Cb*), area postrema (*AP*), and solitary tract nucleus (*Sol*). In other regions the distribution is similar: central gray (*CG*), interpeduncular nucleus (*IPN*), dorsal raphe nucleus (*DR*), and inferior olives (*IO*). Scale bars, 2 mm (scale bar in *g* is for *a–c* and *e–g*; that in *h* is for *d* also).

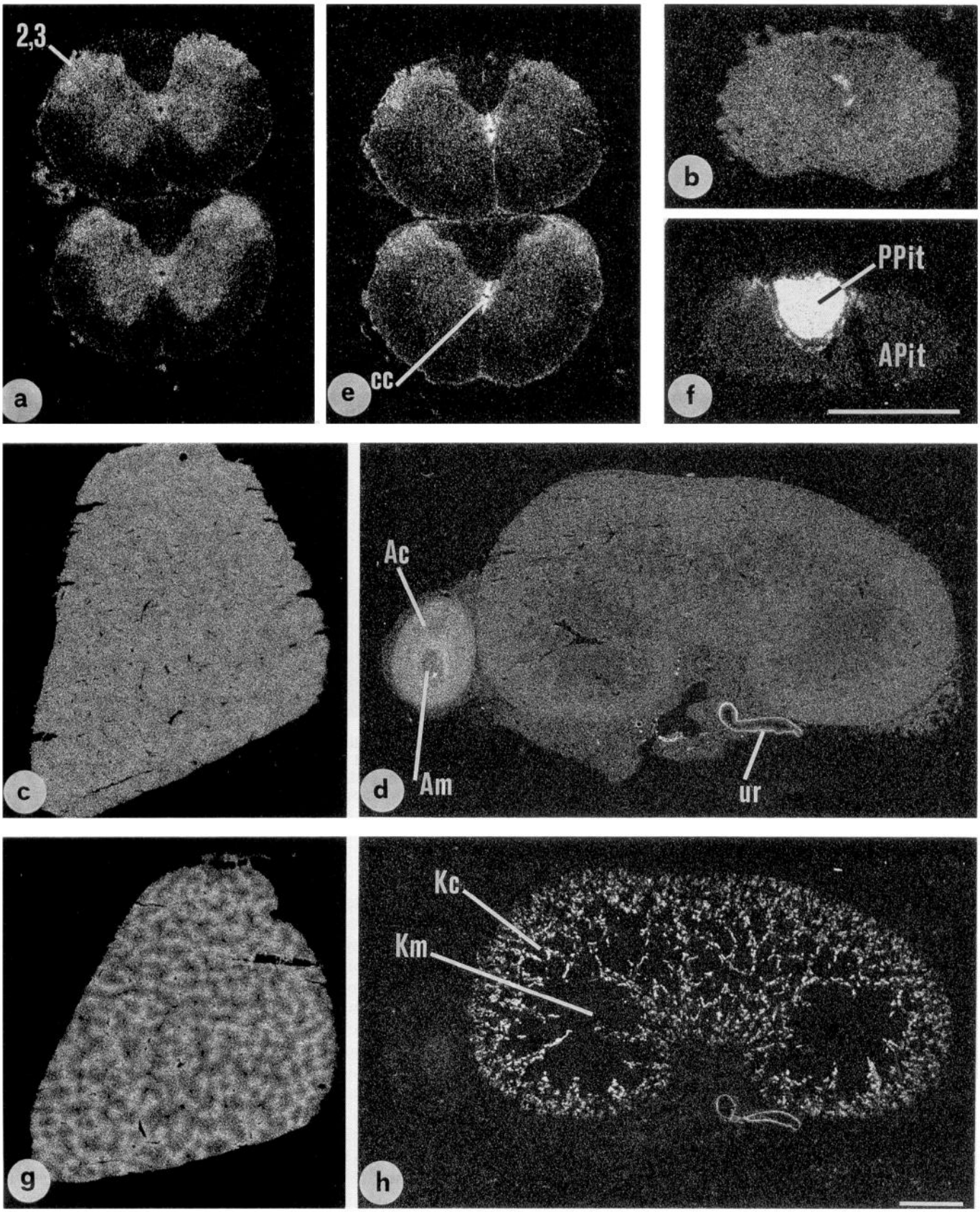

Figure 10. Distribution of the *in vitro* binding sites for ^{3}H-Ro 41-1049 (MAO-A; *a–d*) and ^{3}H-Ro 19-6327 (MAO-B; *e–h*) in adjacent sections of rat spinal cord and peripheral organs under steady state conditions and at [K_D]; macroscopic images, with white areas revealing high binding density. Note the abundance of MAO-B around the central canal (*cc*) of the spinal cord and the presence of both enzymes in layers *2,3* (substantia gelatinosa) of the dorsal horn (*a, e*); the abundance of MAO-B in the posterior lobe of the pituitary (*PPit*) and its virtual absence in the anterior lobe (*APit*) (*b, f*); the abundance of both enzymes in the liver (*c, g*); the presence of MAO-A in the adrenal cortex (*Ac*) and (to a lesser extent) in the adrenal medulla (*Am*) (*d, h*), the abundance of MAO-B in renal tubules of the kidney cortex (*Kc*) but not in the medulla (*Km*) and of both enzymes in the ureter (*ur*). Scale bars, 2 mm.

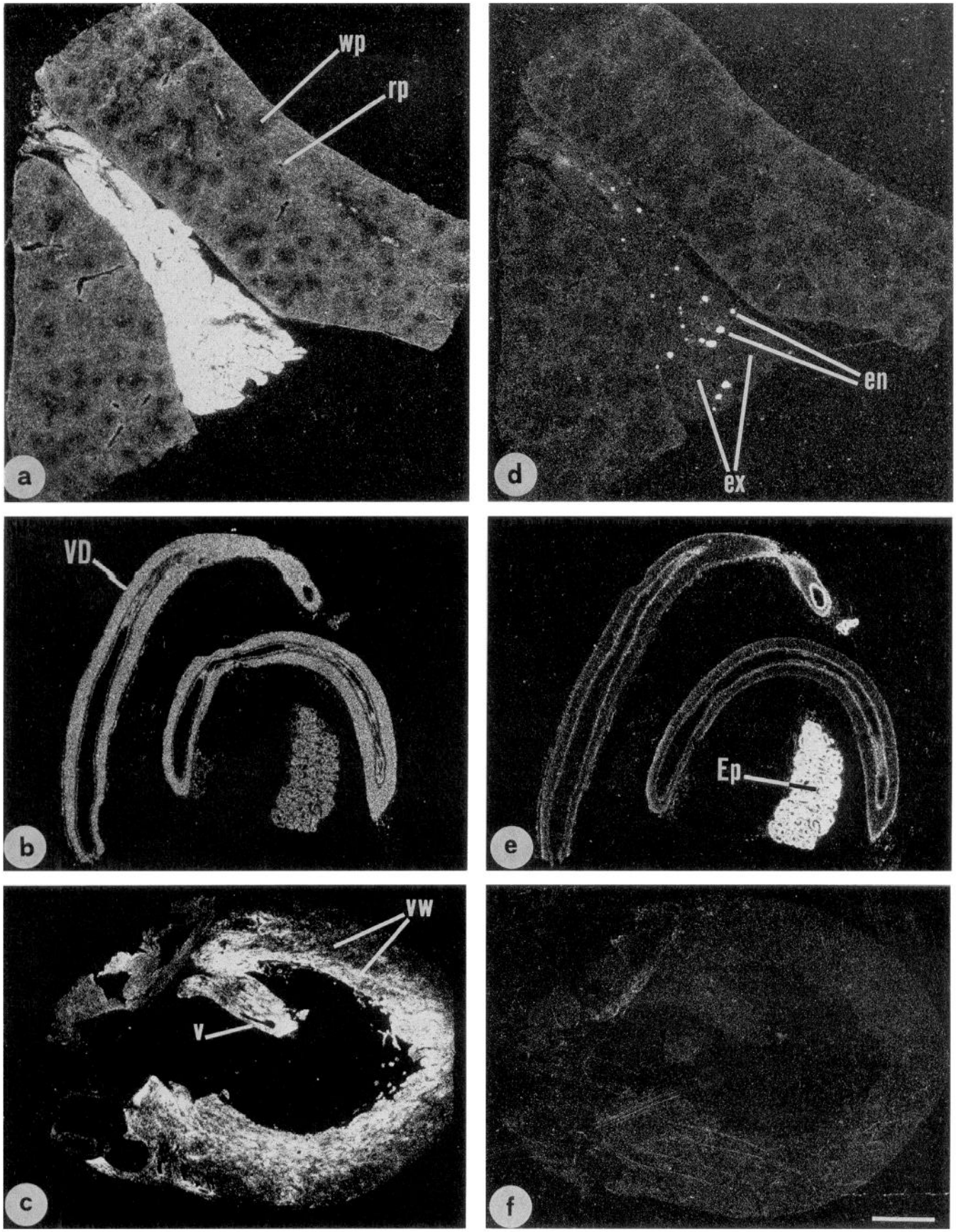

Figure 11. Distribution of the *in vitro* binding sites for ^{3}H-Ro 41-1049 (MAO-A; *a–c*) and ^{3}H-Ro 19-6327 (MAO-B; *d–f*) in adjacent sections of rat peripheral organs under steady state conditions and at [K_D]; macroscopic images, with white areas revealing high binding density. Note the abundance of MAO-A in the exocrine (*ex*) and endocrine (*en*) pancreas and of MAO-B exclusively in the endocrine pancreas (*a, d*); the presence of MAO-A in the red pulp (*rp*) but not in the white pulp (*wp*) of the spleen (*a, d*); the abundance of MAO-A and MAO-B in the vas deferens (*VD*) and epididymis (*Ep*), respectively (*b, e*); and finally, only MAO-A can be detected in the heart [in the ventricle wall (*vw*) and atrioventricular valve (*v*)] (*c, f*). Scale bar, 2 mm.

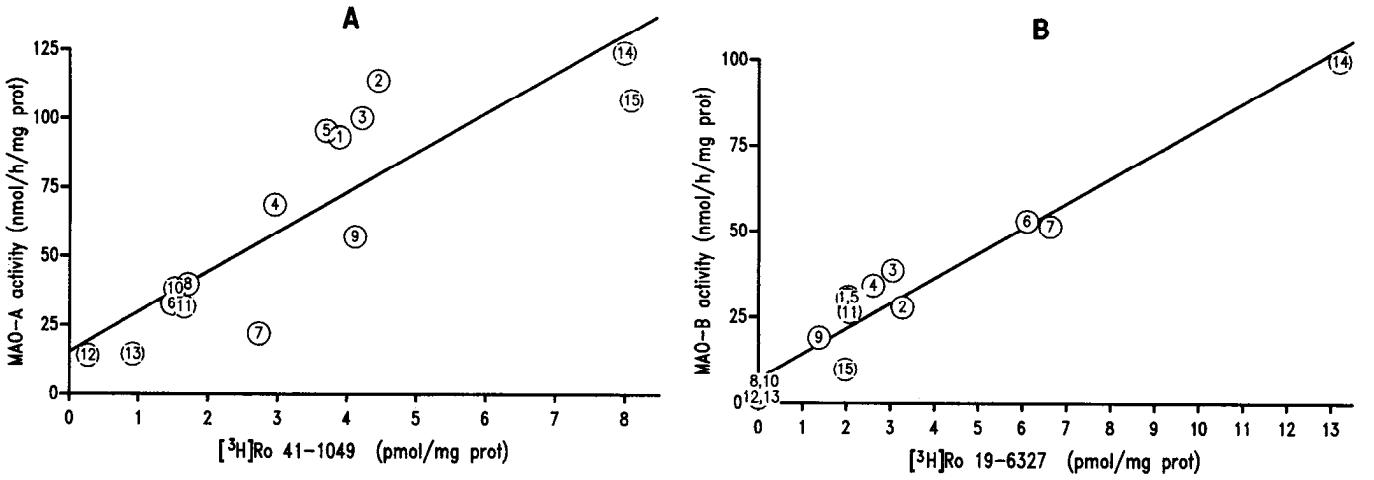

Figure 12. Positive correlations between specific binding of ^{3}H-Ro 41-1049 *in vitro* and MAO-A activity (r = 0.863) (*A*) and between specific binding of ^{3}H-Ro 19-6327 *in vitro* and MAO-B activity (r = 0.968) (*B*) in various rat tissues. Data are from a single experiment (three replicates). *1*, caudate putamen; *2*, nucleus accumbens; *3*, hippocampus; *4*, cerebellum; *5*, cortex; *6*, pineal gland; *7*, posterior lobe pituitary; *8*, heart; *9*, duodenum; *10*, kidney; *11*, lung; *12*, muscle; *13*, spleen; *14*, liver; *15*, superior cervical ganglion.

of MAO-A in the A_6 cell group of the locus coeruleus, in noradrenergic neurons of the pons and medulla, as well as in peripheral nerve fibers (Ryder et al., 1979; Tago et al., 1984; Westlund et al., 1985, 1988; Arai et al., 1986; Kitahama et al., 1986, 1987; Maeda et al., 1987; Thorpe et al., 1987; Konradi et al., 1988, 1989; Willoughby et al., 1988; Shigematsu et al., 1989; May et al., 1991a,b); and (2) recent evidence (Richards et al., 1992) from *in situ* hybridization histochemistry, revealing the presence of MAO-A mRNA (but not MAO-B mRNA) in noradrenergic neurons of the human locus coeruleus.

The lack of MAO-A in serotoninergic neurons despite the assumption that 5-HT is a preferred natural substrate for this enzyme has prompted the suggestion that MAO-A in noradrenergic neurons, in addition to its indirect role in the inactivation of released noradrenaline, might serve a scavenger function by inactivating 5-HT accumulating as a false neurotransmitter (Murphy, 1978; Levitt et al., 1982; Westlund et al., 1988).

MAO-B. A comparison of the distribution, in rat and human brain, of MAO-B (revealed by ^{3}H-Ro 19-6327 binding) with that of tyrosine hydroxylase– and 5-HT–immunoreactive cells and their processes (Hökfelt et al., 1984b; Steinbusch, 1984) and of the glia marker GFAP (glia fibrillary acid protein) (see, e.g., Schmidt-Kastner and Szymas, 1990) suggests that the enzyme is present in astrocytes, ependymal cells, circumventricular organs, and serotoninergic neurons. Glia-rich brain regions such as the olfactory nerve layer (Jaffé and Cuello, 1981), hippocampus (lacunosum moleculare), dentate gyrus (hilus), pial surface, as well as Bergmann glia cells both were intensely stained with an antibody to GFAP and contained a high amount of MAO-B. Whereas MAO-B was consistently found in serotoninergic cell bodies (e.g., dorsal, median, and magnus raphe nuclei), no correlation between brain regions (globus pallidus, substantia nigra) densely innervated by serotoninergic neurons and their MAO-B content could be established (see also Levitt et al., 1982). On the other hand, brain regions (such as the cerebellum) with little or no serotoninergic innervation contained a moderate to high amount of MAO-B.

The presence of MAO-B in serotoninergic neurons, ependyma, circumventricular organs, and astrocytes in rat and human brain is supported by (1) enzyme histochemical and immunohistochemical evidence for the presence of MAO-B in serotoninergic neurons of the raphe nuclei, hypothalamus, pons, and medulla (Ryder et al., 1979; Levitt et al., 1982; Kishimoto et al., 1983; Maeda et al., 1984, 1987; Tago et al., 1984, 1987; Westlund et al., 1985, 1988; Arai et al., 1986; Kitahama et al., 1986, 1987, 1989; Thorpe et al., 1987; Konradi et al., 1988, 1989; Willoughby et al., 1988); (2) similar evidence for the presence of MAO-B in astrocytes (Levitt et al., 1982; Nakamura et al., 1990) and in circumventricular organs (Levitt et al., 1982); (3) evidence from radioautographical investigations with ^{3}H-pargyline, ^{3}H- and ^{11}C-L-deprenyl, and ^{3}H-MPTP (1-methyl-4-phenyl-1,2,5,6-tetrahydropyridine; Javitch et al., 1984; Parsons and Rainbow, 1984; Rainbow et al., 1985; Reznikoff et al., 1985; Jossan et al., 1989, 1990; May et al., 1991a,b); (4) evidence from PET studies using ^{11}C-deprenyl (Fowler et al., 1987); (5) enzyme histochemical studies using MPTP as substrate (Nakamura and Vincent, 1986); and (6) recent evidence (Richards et al., 1992) from *in situ* hybridization histochemistry revealing the presence of mRNA coding for MAO-B (but not MAO-A) in serotoninergic neurons of the human raphe.

Although dopamine is known to have a twofold higher affinity *in vitro* for MAO-A than MAO-B in rat brain but an equal affinity for the enzymes in human brain, their *in vivo* affinities are not known. Consequently, the physiological role of MAO-B (and MAO-A) in the metabolism of dopamine, if any, is yet to be clarified.

The role of MAO-B in serotoninergic neurons might be to prevent the cells from accumulating various natural substrates (e.g., dopamine), which could interfere with the storage, release uptake, and receptor function of 5-HT (Murphy, 1978; Levitt et al., 1982; Westlund et al., 1988). The physiological role of MAO-B in cells of the ependyma and most circumventricular organs (except the choroid plexus, where there the enzyme is lacking) might be to protect the brain from the variety of trace amines (phenethylamine, tryptamine, methylhistamine) that are assumed to be preferred natural substrates for the enzyme. The role of MAO-B in astrocytes might be dual: (1) in the vicinity of monoaminergic nerve terminals, to metabolize released transmitters taken up, and (2) throughout the brain, to inactivate

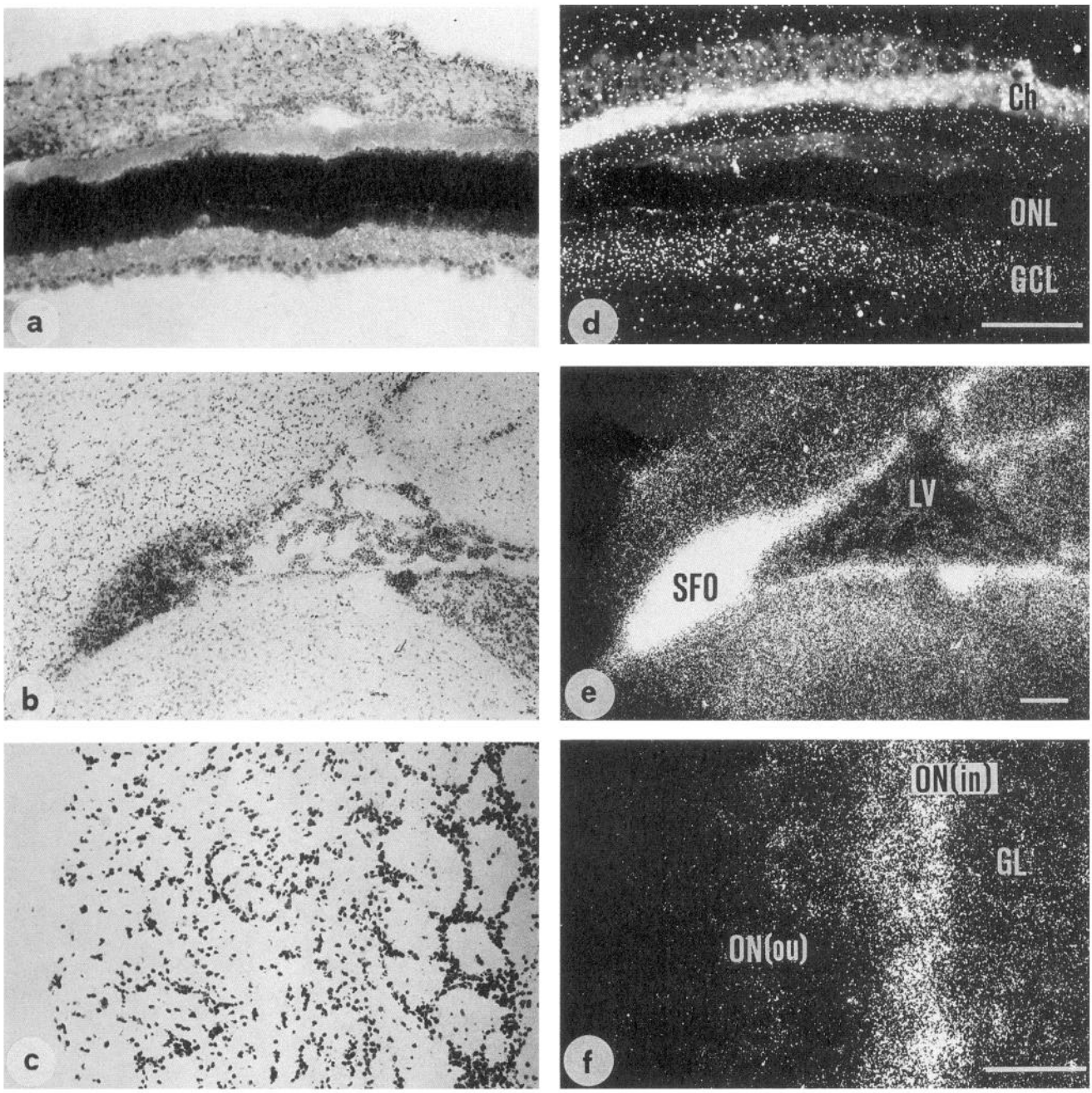

Figure 13. Microscopic localization of MAO-A (*d*) and MAO-B (*e, f*) binding sites in various rat tissues revealed by bright-field optics (*a–c*) and the appearance of white silver grains in dark-field optics (*d–f*). Hematoxylin-eosin staining (except *b* and *c*, cresyl violet). Note the abundance of MAO-A in the ganglion cell layer of the retina (*GCL, d*) and of MAO-B in the subfornical organ (*SFO, e*) and inner olfactory nerve layer [*ON(in), f*]. *Ch,* choroid; *ONL,* outer nuclear layer; *LV,* lateral ventricle; *ON(ou),* outer olfactory nerve layer; *GL,* glomerular layer. Scale bars, 200 μm.

trace amines that could otherwise be accumulated by neuronal uptake to also act as false neurotransmitters or to displace the physiological transmitter from their vesicular stores.

It is perhaps worth pointing out that the MAO-B–rich hypothalamic neurons (of the latero- and tuberomamillary nuclei) in human and rat brain (Levitt et al., 1982; Westlund et al., 1988) might not be serotoninergic but histaminergic (Steinbusch and Mulder, 1984; Bayliss et al., 1990). Methylhistamine is an excellent substrate for MAO-B both *in vitro* and *in vivo* (Dostert et al., 1989). The histaminergic nature of these MAO-B–positive neurons in the human brain was recently demonstrated by *in situ* hybridization histochemistry using ^{35}S-labeled oligonucleotide probes for MAO-B and histidine decarboxylase (Saura et al., in preparation).

The fact that there exist species differences in enzyme activity [rat heart MAO-A ≫ MAO-B vs. human heart MAO-B > MAO-A (Haenick et al., 1981); choroid plexus MAO-B mouse ≫ rat] and enzyme substrates (whereas in rat brain dopamine is a preferential substrate for MAO-A, in human brain it is a substrate for both enzymes) (Waldmeier et al., 1976; O'Carroll et al., 1983) complicates the interpretation of the physiological roles these enzymes play in specific brain regions of different

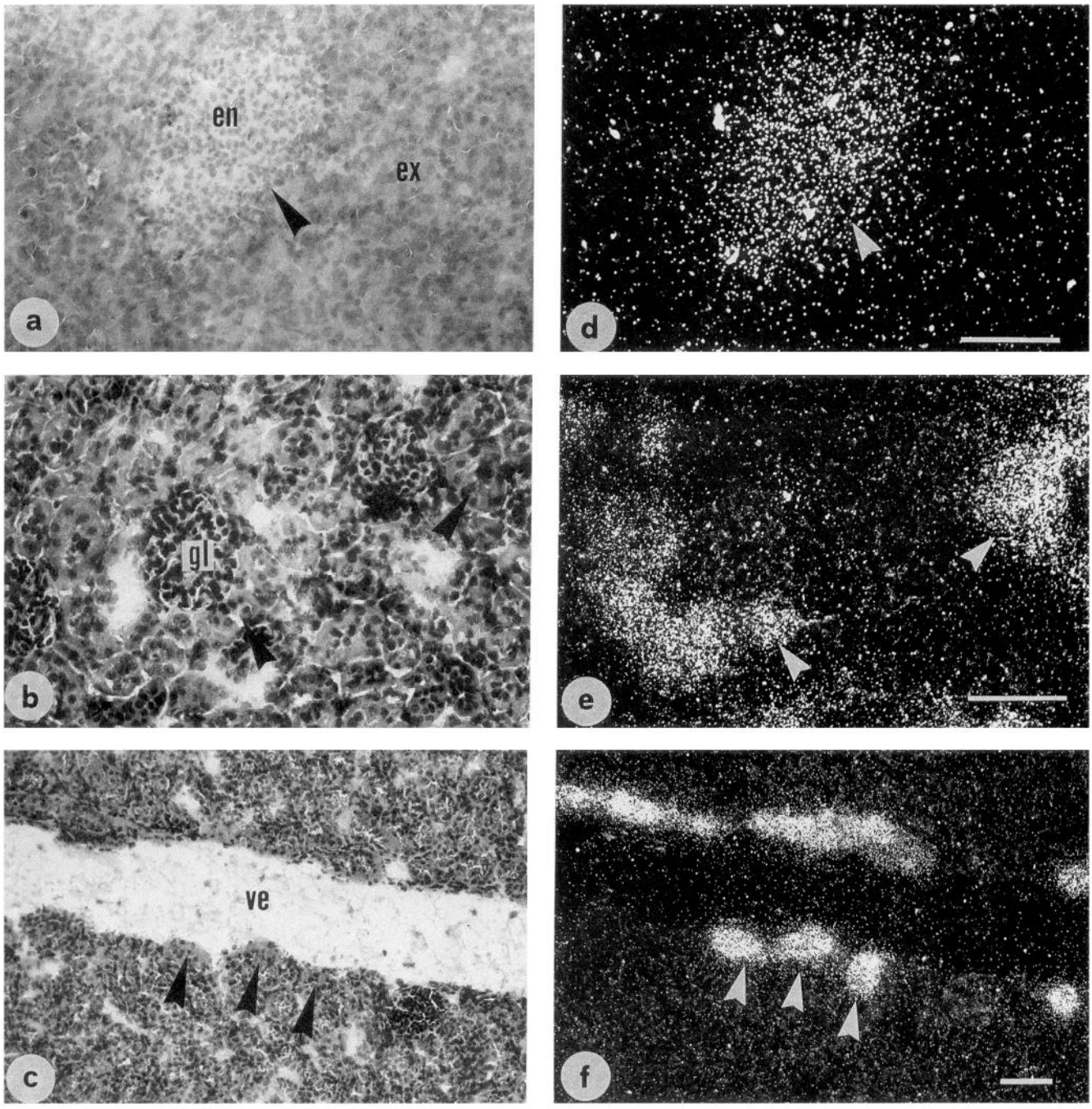

Figure 14. Microscopic localization of MAO-B binding sites in various rat tissues revealed by bright-field optics (*a–c*) and the appearance of white silver grains in dark-field optics (*d–f*). Hematoxylin-eosin staining. Note the abundance of MAO-B in endocrine pancreas (*en*) (*a* and *d, arrowheads*) and kidney tubules of the renal cortex and vein (*ve*) (*arrowheads, b, c, e,* and *f*). *ex,* exocrine pancreas; *gl,* glomerulus. Scale bars, 100 μm.

→

Figure 15. Distribution of the *in vitro* binding sites for ^{3}H-Ro 41-1049 (MAO-A; *a–c*) and ^{3}H-Ro 19-6327 (MAO-B; *d–f*) in adjacent sections of human postmortem brain and spinal cord under steady state conditions at at [K_D]; macroscopic images, with white areas revealing high binding density. Note the abundance of MAO-B in the polymorphic layer of the hilus in the dentate gyrus (*DG*) and in the *CA3* pyramidal layer of the hippocampus (*d*); the presence of both MAO-A and MAO-B (the former more discrete) in the substantia nigra (*SNc,* pars compacta; *SNr,* pars reticulata; *b, e*); the presence of both enzymes (MAO-B more discrete) in the dorsal and central raphe nuclei (*NRD, NRC*) and the abundance of MAO-B in the ependyma (*ep*) lining the aqueduct (*AQ*) and of MAO-A in the locus coeruleus (*LC*) (*c, f*). *f,* fimbria; *S,* subiculum; *CA1,* hippocampal region. Scale bars, 200 μm.

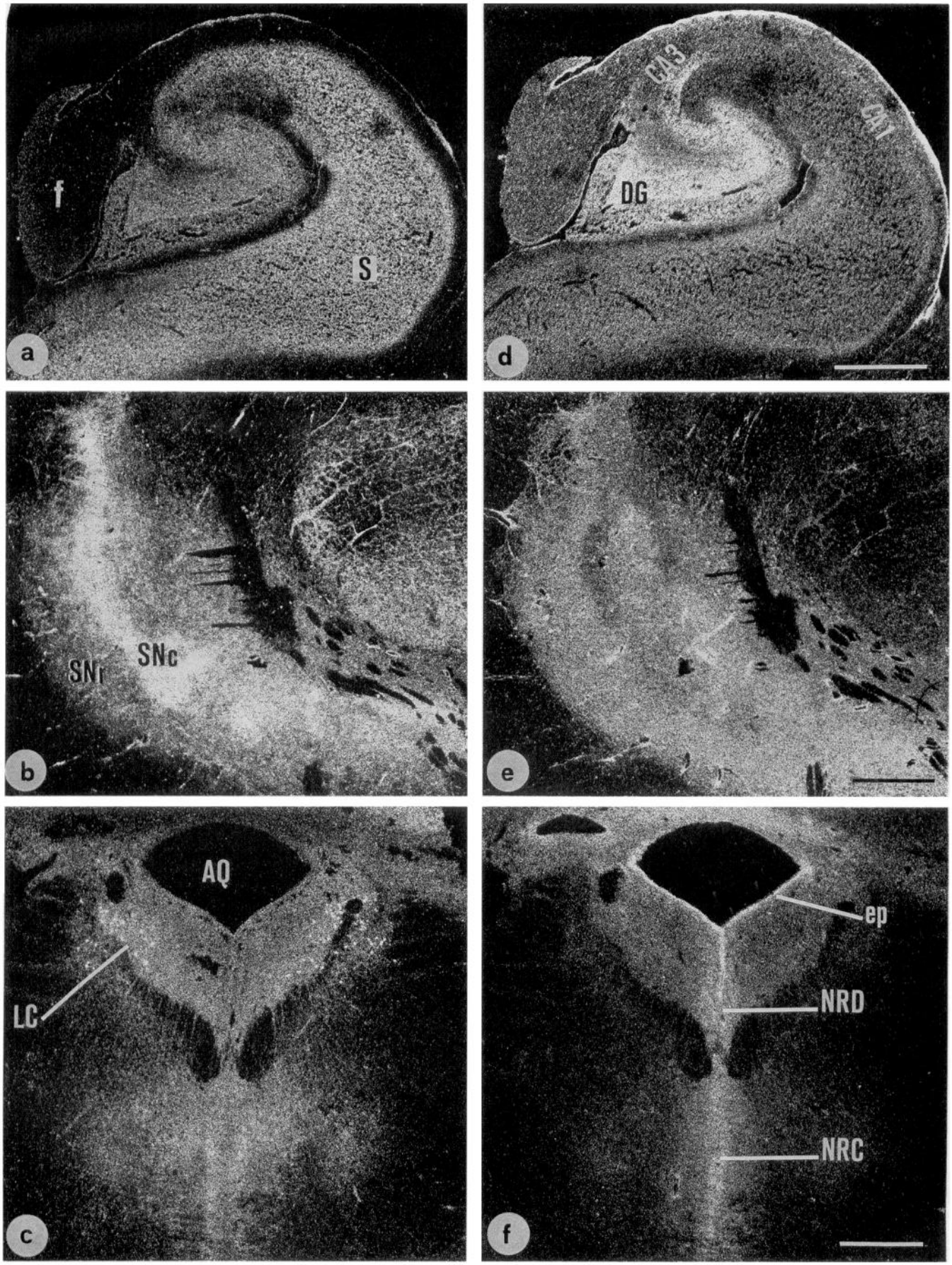
f
S
a
CA3
CA1
DG
d
SNr
SNc
b
e
AQ
LC
c
ep
NRD
NRC
f

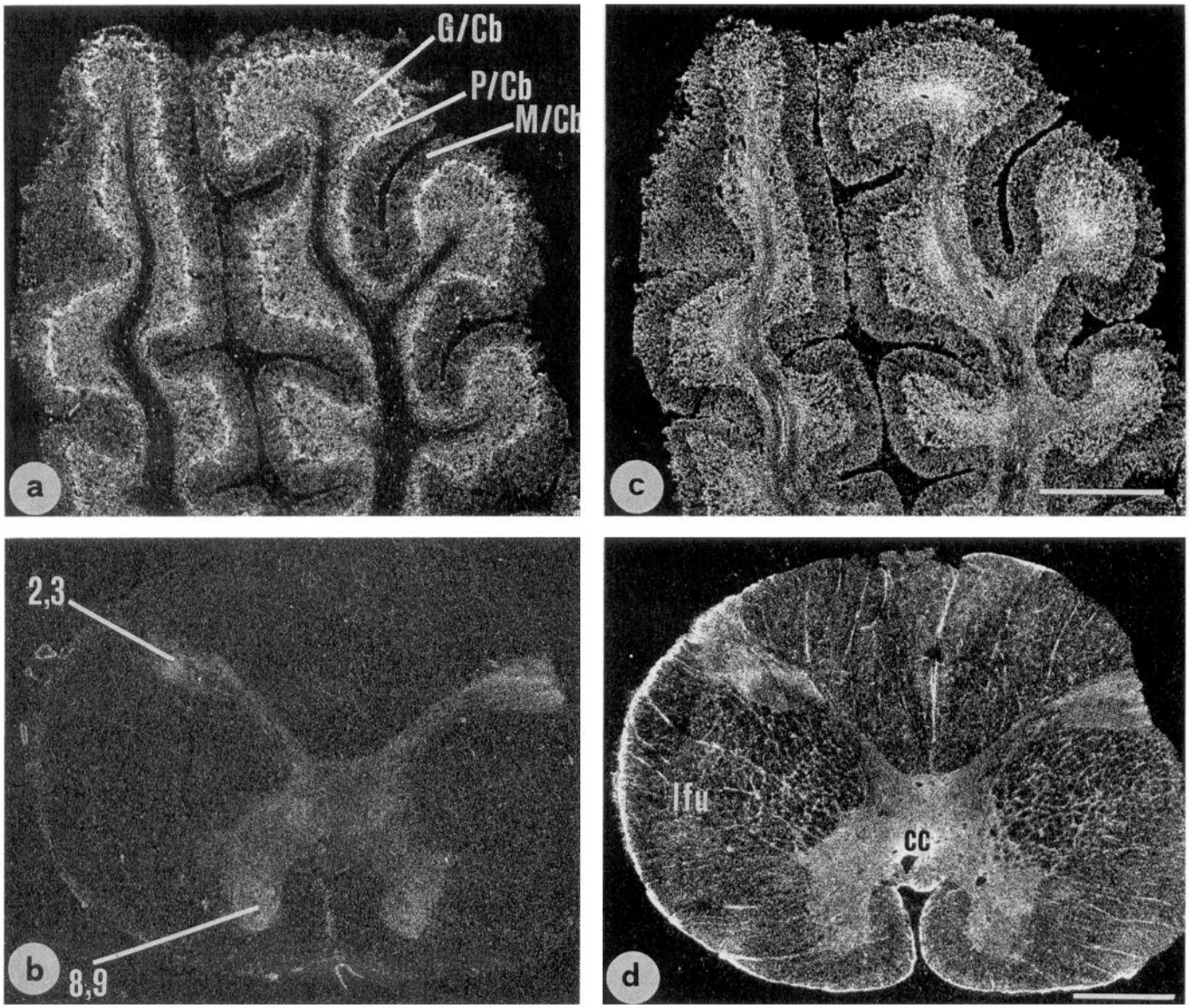

Figure 16. Distribution of the *in vitro* binding sites for ^{3}H-Ro 41-1049 (MAO-A; *a, b*) and ^{3}H-Ro 19-6327 (MAO-B; *c, d*) in adjacent sections of human postmortem brain and spinal cord under steady state conditions and at [K_D]; macroscopic images, with white areas revealing high binding density. Note the presence of MAO-A in the cerebellar Purkinje cell layer (*P/Cb, a*) and the presence of both enzymes (MAO-A more discrete) in layers of the dorsal (*2,3*) and ventral (*8,9*) horns of the spinal cord (*b, d*). MAO-B is also abundant around the central canal (*cc*). *G/Cb,* cerebellar granular layer; *M/Cb,* cerebellar molecular layer; *lfu,* lateral funiculus. Scale bars, 200 μm.

species. It also makes it difficult to predict from animal studies the relevance to the situation in human brain.

Conclusions and future perspectives

The results presented in this article provide the first quantitative analysis of the distribution and abundance of MAO-A and MAO-B in discrete regions of the rat CNS, peripheral organs, and human postmortem brain by enzyme radioautography.

Many applications of this sensitive and highly selective technique might be envisaged, for example, for investigations of the pharmacological, developmental, or pathophysiological regulation of these enzymes and their rates of *de novo* synthesis. Differential age-related changes (Strolin Benedetti and Kaene, 1980; Arai et al., 1985; Meco et al., 1987; Arai and Kinemuchi, 1988; Strolin Benedetti and Dostert, 1989; Konradi et al., 1990) and disease-related changes (Gottfries et al., 1983; Oreland and Gottfries, 1986; Gottfries, 1988; Reinikanen et al., 1988; Jossan et al., 1990; Nakamura et al., 1990) in the enzymes have been reported in the literature that could indicate a therapeutic potential for MAO inhibitors in neurodegenerative diseases.

References

Abel CW, Denney RM, Westlund KN (1988) Localization and function of monoamine oxidases A and B. In: Progress in catecholamine research, Pt A, Basic aspects and peripheral mechanisms (Dahlström A, Belmarker RH, Sandler M, eds), pp 103–108. New York: Liss.

Arai R, Kimura H, Maeda T (1986) Topographic atlas of monoamine oxidase-containing neurons in the rat brain studied by an improved histochemical method. Neuroscience 19:905–925.

Arai Y, Kinemuchi H (1988) Differences between MAO concentra-

tions in striatum and forebrain of aged and young rats. J Neural Transm 72:99–105.
Arai Y, Stenström A, Oreland L (1985) The effect of age on intra- and extraneuronal monoamine oxidase-A and -B activities in the rat brain. Biog Amines 2:65–71.
Bach AWJ, Lan NC, Johnson DL, Abell CW, Bembenek ME, Kwan SW, Seeburg P, Shih JC (1988) cDNA cloning of human liver monoamine oxidase A and B: molecular basis of differences in enzymatic properties. Proc Natl Acad Sci USA 85:4934–4938.
Bayliss DA, Wang Y-M, Zahnow CA, Joseph DR, Millhorn DE (1990) Localization of histidine decarboxylase mRNA in rat brain. Mol Cell Neurosci 1:3–9.
Björklund A, Lindvall O (1984) Dopamine-containing systems in the CNS. In: Handbook of chemical neuroanatomy, Vol 2, Classical transmitters in the CNS, Pt I (Björklund A, Hökfelt T, eds), pp 55–122. Amsterdam: Elsevier.
Blaschko H, Richter D, Schlossmann H (1937) The inactivation of adrenaline. J Physiol (Lond) 90:1–17.
Burkard WP, Bonetti EP, Da Prada M, Martin JR, Polc P, Schaffner R, Scherschlicht R, Hefti F, Müller RKM, Wyss P-C, Haefely W (1989) Pharmacological profile of moclobemide, a short-acting and reversible inhibitor of monoamine oxidase type A. J Pharmacol Exp Ther 248:391–399.
Cesura AM, Galva MD, Imhof R, Kyburz E, Picotti GB, Da Prada M (1989) [^{3}H]Ro 19-6327: a reversible ligand and affinity labelling probe for monoamine oxidase-B. Eur J Pharmacol 162:457–465.
Cesura AM, Bös M, Galva MD, Imhof R, Da Prada M (1990) Characterization of the binding of [^{3}H]Ro 41-1049 to the active site of human monoamine oxidase-A. Mol Pharmacol 37:358–366.
Chai SY, McKenzie JS, McKinley MJ, Mendelsohn FAO (1990) Angiotensin converting enzyme in the human basal forebrain and midbrain visualized by *in vitro* autoradiography. J Comp Neurol 291: 179–194.
Da Prada M, Kettler R, Keller HH, Burkard WP, Muggli-Maniglio D, Haefely WE (1989a) Neurochemical profile of moclobemide, a short-acting and reversible inhibitor of monoamine oxidase type A. J Pharmacol Exp Ther 248:400–414.
Da Prada M, Kettler R, Keller HH, Burkard WP, Haefely WE (1989b) Preclinical profiles of the novel reversible MAO-A inhibitors, moclobemide and brofaromine, in comparison with irreversible MAO inhibitors. J Neural Transm [Suppl] 28:5–20.
Da Prada M, Kettler R, Burkard WP, Lorez HP, Haefely W (1990a) Some basic aspects of reversible inhibitors of monoamine oxidase-A. Acta Psychiatry Scand 92: [Suppl 360] 7–12.
Da Prada M, Kettler R, Keller HH, Cesura AM, Richards JG, Saura Marti J, Muggli Maniglio D, Wyss P-C, Kyburz E, Imhof R (1990b) From moclobemide to Ro 19-6327 and Ro 41-1049: the development of a new class of reversible, selective MAO-A and MAO-B inhibitors. J Neural Transm [Suppl] 29:179–192.
De Armond SJ, Fusco MM, Dewey MM (1989) Structure of the human brain. A photographic atlas, 3d ed. Oxford: Oxford UP.
Denney RM, Denney CB (1985) An update on the identity crisis of monoamine oxidase: new and old evidence for the independence of MAO A and B. Pharmacol Ther 30:227–259.
Dostert PL, Strolin Benedetti M, Tipton KF (1989) Interactions of monoamine oxidase with substrates and inhibitors. Med Res Rev 9: 45–89.
Fowler CJ, Oreland L, Marcusson J, Winblad R (1980) Titration of human brain monoamine oxidase-A and -B by clorgyline and L-deprenyl. Naunyn Schmiedebergs Arch Pharmacol 311:263.
Fowler JS, MacGregor RR, Wolf AP, Arnett CD, Dewey SL, Schyler D, Christman D, Logan J, Smith M, Sachs H, Aquilonius SM, Njurling P, Halldin C, Hartvig P, Leenders KL, Lundqvist H, Oreland L, Stalnacke CG, Langstrom B (1987) Mapping human brain MAO-A and -B with ^{11}C-labeled suicide inactivators and PET. Science 23: 481–485.
Glenner GG, Burtner HJ, Brown GW (1957) The histochemical demonstration of monoamine oxidase activity by tetrazolium salts. J Histochem Cytochem 5:591–600.
Glover V, Sandler M (1987) Monoamine oxidase and the brain. Rev Neurosci 1:145–156.
Gottfries CG (1988) Alzheimer's disease. Compr Gerontol 2:47–62.
Gottfries CG, Adolfsson R, Aquilonius S-M, Carlsson A, Eckernäs S-Å, Nordberg A, Oreland L, Svennerholm L, Wiberg Å, Winblad B (1983) Biochemical changes in dementia disorders of Alzheimer type (AD/SDAT). Neurobiol Aging 4:261–271.
Graham RC, Karnovsky MJ (1965) The histochemical demonstration of monoamine oxidase by coupled peroxidatic oxidation. J Histochem Cytochem 13:604–605.
Grimsby J, Chen K, Wang L-J, Lan NC, Shih JC (1991) Human monoamine oxidase A and B genes exhibit identical exon-intron organization. Proc Natl Acad Sci USA 88:3637–3641.
Haefely W, Kettler R, Keller HH, Da Prada M (1990) Ro 19-6327, a reversible and highly selective monoamine oxidase B inhibitor: a novel tool to explore the MAO-B function in humans. In: Advances in neurology, Vol 53, Parkinson's disease: anatomy, pathology, and therapy (Streifler MB, Korczyn AD, Melamed E, Youdim MBH, eds), pp 505–512. New York: Raven.
Haefely W, Burkard WP, Cesura AM, Kettler R, Lorez HP, Martin JR, Richards JG, Scherschlicht R, Da Prada M (1992) Biochemistry and pharmacology of moclobemide, a prototype R.I.M.A. Psychopharmacol 106:S6–S14.
Haenick D, Boehme DH, Vogel WH (1981) Monoamine oxidase in four rat and human tissues. Biochem Med 26:451–454.
Heikkila RE, Terleckyj I, Sieber BA (1990) Monoamine oxidase and the bioactivation of MPTP and related neurotoxins: relevance to DATATOP. J Neural Transm 32: [Suppl] 217–227.
Hökfelt T, Johansson O, Goldstein M (1984a) Central catecholamine neurons as revealed by immunohistochemistry with special reference to adrenaline neurons. In: Handbook of chemical neuranatomy, Vol 2, Classical transmitters in the CNS, Pt I (Björklund A, Hökfelt T, eds), pp 157–276. Amsterdam: Elsevier.
Hökfelt T, Mårtensson R, Björklund A, Kleinau S, Goldstein M (1984b) Distributional maps of tyrosine-hydroxylase-immunoreactive neurons in the rat brain. In: Handbook of chemical neuroanatomy, Vol 2, Classical transmitters in the CNS, Pt I (Björklund A, Hökfelt T, eds), pp 277–379. Amsterdam: Elsevier.
Ito A, Kuwahara T, Inadome S, Sagara Y (1988) Molecular cloning of a cDNA for rat liver monoamine oxidase B. Biochem Biophys Res Commun 157:970–976.
Jaffé EH, Cuello AC (1981) Neuronal and glial release of [^{3}H]GABA from the rat olfactory bulb. J Neurochem 37:1457–1466.
Javitch JA, Uhl GR, Snyder SH (1984) Parkinsonism-inducing neurotoxin, *N*-methyl-4-phenyl,1,2,3,6-tetrahydropyridine: characterization and localization of receptor binding sites in rat and human brain. Proc Natl Acad Sci USA 81:4591–4595.
Johnston JP (1968) Some observations upon a new inhibitor of monoamine oxidase in brain tissue. Biochem Pharmacol 17:1285–1297.
Jossan SS, d'Argy R, Gillberg PG, Aquilonius SM, Långström B, Halldin C, Bjurling P, Stålnacke CG, Fowler J, MacGregor R, Oreland L (1989) Localization of monoamine oxidase B in human brain by autoradiographical use of ^{11}C-labeled L-deprenyl. J Neural Transm 77:55–64.
Jossan SS, Gillberg P-G, Karlsson I, Gottfries CG, Oreland L (1990) Visualization of brain monoamine oxidase B (MAO-B) in dementia of Alzheimer's type by means of large cryosection autoradiography; a pilot study. J Neurotransm [Suppl] 32:61–66.
Juorio AV (1988) Brain trace amines: mapping studies and effects of mesencephalic lesions. In: Trace amines: comparative and clinical neurobiology (Boulton AA, Juorio AV, Downer RGH, eds), pp 157–174. Clifton, NJ: Humana.
Kettler R, Da Prada M (1989) Platelet MAO-B activity in humans and stumptail monkeys: *in vivo* effects of the reversible MAO-B inhibitor Ro 19-6327. In: Early diagnosis and preventive therapy of Parkinson's disease (Przuntek H, Riederer P, eds), pp 213–219. Berlin: Springer.
Kettler R, Kyburz E, Keller HH, Muggli D, Da Prada M (1989) Neuropharmacological comparison of moclobemide with the novel MAO inhibitor Ro 41-1049 in the rat. Paper presented at the 12th ISN Biennal Meeting 1989, Algarve, Portugal, April 23–28.
Kirchgessner AL, Pintar JE (1991) Guinea pig pancreatic ganglia: projections, transmitter content, and the type-specific localization of monoamine oxidase. J Comp Neurol 305:613–631.
Kishimoto S, Kimura H, Maeda T (1983) Histochemical demonstration for monoamine oxidase (MAO) by a new coupled peroxidation method. Cell Mol Biol 29:61–69.
Kitahama K, Arai R, Maeda T, Jouvet M (1986) Demonstration of MAO-B in serotonergic and MAO-A in noradrenergic neurons in the cat dorsal pontine tegmentum by an improved histochemical technique. Neurosci Lett 71:19–24.
Kitahama K, Kimura H, Maeda T, Jouvet M (1987) Distribution of two types of monoamine oxidase-containing neurons in the cat me-

dulla oblongata demonstrated by an improved histochemical method. Neuroscience 20:991–999.
Kitahama K, Sallanon M, Lin J-S, Maeda T, Jouvet M (1989) Type B monoamine oxidase-containing cells and fibers in the cat hypothalamus demonstrated by an improved enzyme histochemical method. J Comp Neurol 285:218–230.
Knoll J, Magyar K (1972) Some puzzling pharmacological effects of monoamine oxidase inhibitors. Adv Biochem Psychopharmacol 5: 393–408.
Konradi C, Svoma E, Jellinger K, Riederer P, Denney P, Thibault J (1988) Topographic immunocytochemical mapping of MAO-A, MAO-B and tyrosine hydroxylase in human post mortem brain stem. Neuroscience 26:791–802.
Konradi C, Kornhuber J, Froelich L, Fritze J, Heinsen H, Beckmann H, Schulz E, Riederer P (1989) Demonstration of monoamine oxidase-A and -B in the human brainstem by a histochemical technique. Neuroscience 33:383–400.
Konradi C, Riederer P, Heinsen H (1990) Histochemistry of MAO subtypes in the brainstem of humans: a relation to the radical hypothesis of Parkinson's disease? In: Early diagnosis and preventive therapy in Parkinson's disease (Przuntek H, Riederer P, eds), pp 243–248. Berlin: Springer.
Kuhar MJ, Unnerstall JR (1990) Receptor autoradiography. In: Methods in neurotransmitter receptor analysis (Yamamura HI, Enna SJ, Kuhar MJ, eds), pp 177–218. New York: Raven.
Kuwahara T, Takamoto S, Ito A (1990) Primary structure of rat monoamine oxidase A deduced from cDNA and its expression in rat tissues. Agric Biol Chem 54:253–257.
Levitt P, Pintar JE, Breakfield XO (1982) Immunocytochemical demonstration of MAO-B in brain astrocytes and serotonergic neurons. Proc Natl Acad Sci USA 79:6385–6389.
Maeda T, Kimura H, Nagai T, Imai H, Arai R, Sakumoto T, Sakai K, Kitahama K, Jouvet M (1984) Histochemistry of the magnocellular neurons in the posterior hypothalamus, with special reference to MAO activity and ability of 5HTP uptake and decarboxylation. Acta Histochem Cytochem 17:179–193.
Maeda T, Imai H, Arai R, Tago H, Nagai T, Sakumoto T, Kitahama K, Onteniente B, Kimura H (1987) An improved coupled peroxidatic oxidation method of MAO histochemistry for neuroanatomical research at light and electron microscopic levels. Cell Mol Biol 33:1–11.
May T, Rommelspacher H, Pawlik M (1991a) [^{3}H]harman binding experiments. I: A reversible and selective radioligand for monoamine oxidase subtype A in the CNS of the rat. J Neurochem 56:490–499.
May T, Pawlik M, Rommelspacher H (1991b) [^{3}H]harman binding experiments. II: Regional and subcellular distribution of specific [^{3}H]harman binding and monoamine oxidase subtypes A and B activity in marmoset and rat. J Neurochem 56:500–508.
McPherson GA (1985) Analysis of radioligand binding experiments. J Pharmacol Methods 14:213–228.
Meco M, Bonifati V, Collier WL, Ramacci MT, Amenta F (1987) Enzyme histochemistry of MAO in the heart of aged rats. Mech Ageing Dev 38:145–155.
Moll G, Moll R, Riederer P, Gsell W, Heinsen H, Denney RM (1990) Immunofluorescence cytochemistry on thin frozen sections of human substantia nigra for staining of monoamine oxidase A and monoamine oxidase B: a pilot study. J Neural Transm [Suppl] 32:67–77.
Moore RY, Card P (1984) Noradrenaline-containing neuron systems. In: Handbook of chemical neuroanatomy, Vol 2, Classical transmitters in the CNS, Pt I (Björklund A, Hökfelt T, eds), pp 123–156. Amsterdam: Elsevier.
Murphy DL (1978) Substrate-selective monoamine oxidases. Biochem Pharmacol 27:1889–1893.
Nakamura S, Vincent SR (1986) Histochemistry of MPTP oxidation in the rat brain: sites of synthesis of the Parkinsonism-inducing toxin MPP$^+$. Neurosci Lett 65:321–325.
Nakamura S, Kawamata T, Akiguchi I, Kameyama M, Nakamura N, Kimura H (1990) Expression of monoamine oxidase B activity in astrocytes of senile plaques. Acta Neuropathol (Berl) 80:319–325.
Nieuwenhuys R, Voogd J, van Huijzen C (1988) The human central nervous system. A synopsis and atlas, 3d ed. Berlin: Springer.
O'Carroll A-M, Fowler CJ, Phillips JP, Tobbia I, Tipton KF (1983) The deamination of dopamine by human brain monoamine oxidase specificity for the two enzyme forms in seven brain regions. Naunyn Schmiedebergs Arch Pharmacol 322:198–202.
Oreland L, Gottfries CG (1986) Brain monoamine oxidase in aging and in dementia of Alzheimer type. Prog Neuropsychopharmacol Biol Psychiatr 10:533–540.
Parkinson study group (1989a) Effect of deprenyl on the progression of disability in early Parkinson's disease. N Engl J Med 321:1364–1371.
Parkinson study group (1989b) DATATOP: a multicenter controlled clinical trial in early Parkinson's disease. Arch Neurol 46:1052–1060.
Parsons B, Rainbow TC (1984) High-affinity binding sites for ^{3}H-MPTP may correspond to MAO. Eur J Pharmacol 102:375–377.
Paxinos G, ed (1990) The human nervous system. San Diego: Academic.
Paxinos G, Watson C, eds (1986) The rat brain in stereotaxic coordinates, 2nd ed. San Diego: Academic.
Pintar JE, Levitt P, Salach JI, Weyler W, Rosenberg MB, Breakfield XO (1983) Specificity of antisera prepared against pure bovine MAO-B. Brain Res 276:127–139.
Rainbow TC, Parsons B, Wieczorek CM, Manaker S (1985) Localization in rat brain of binding sites for parkinsonian toxin MPTP: similarities with ^{3}H-pargyline binding to MAO. Brain Res 330:337–343.
Reinikanen KJ, Paljärvi L, Halonen T, Malminen O, Kosma V-M, Laakso M, Riekkinen PJ (1988) Dopaminergic system and monoamine oxidase-B activity in Alzheimer's disease. Neurobiol Aging 9: 245–252.
Reznikoff G, Manaker S, Parsons B, Harker Rhodes C, Rainbow TC (1985) Similar distribution of monoamine oxidase (MAO) and parkinsonian toxin (MPTP) binding sites in human brain. Neurology 35: 1415–1419.
Richards JG, Saura Marti J, Cesura AM, Da Prada M (1988) Quantitative enzyme radioautography with [^{3}H]Ro 19-6327: localization of MAO-B in rat CNS, peripheral organs and human brain. Pharmacol Res Commun 20: [Suppl IV] 91–92.
Richards JG, Saura J, Ulrich J, Da Prada M (1992) Molecular neuroanatomy of monoamine oxidases. Psychopharmacol 106:S21–S23.
Riederer P, Konradi C, Youdim MBH (1990) The role of MAO in dopaminergic transmission. Arch Neurol 53:149–153.
Ryder TA, McKenzie ML, Pryse-Davies J, Glover V, Lewinsohn R, Sandler M (1979) A coupled peroxidatic oxidation technique for the histochemical localization of monoamine oxidase A and B and benzylamine oxidase. Histochemistry 62:93–100.
Saura Marti J, Kettler R, Da Prada M, Richards JG (1990a) Selective inhibition of MAO-B in rat brain by Ro 19-6327: correlation with binding *in vivo*. Br J Pharmacol [Proc Suppl] 99:69P.
Saura Marti J, Kettler R, Da Prada M, Richards JG (1990b) Molecular neuroanatomy of MAO-A and MAO-B. J Neural Transm [Suppl] 32: 49–53.
Schmidt-Kastner R, Szymas J (1990) Immunohistochemistry of glial fibrillary acidic protein, vimentin and S-100 protein for study of astrocytes in hippocampus of rat. J Chem Neuroanat 3:179–192.
Shigematsu K, Akiguchi I, Oka N, Kamo H, Matsubayashi K, Kameyama M, Kawamura J, Maeda T (1989) Monoamine oxidase-containing nerve fibers in the major cerebral arteries of rats. Brain Res 497:21–29.
Steinbusch HWM (1984) Serotonin-immunoreactive neurons and their projections in the CNS. In: Handbook of chemical neuroanatomy, Vol 2, Classical transmitters in the CNS, Pt I (Björklund A, Hökfelt T, eds), pp 68–125. Amsterdam: Elsevier.
Steinbusch HWM, Mulder AH (1984) Immunohistochemical localization of histamine in neurons and mast cells in the rat brain. In: Handbook of chemical neuroanatomy, Vol 2, Classical transmitters in the CNS, Pt I (Björklund A, Hökfelt T, eds), pp 126–140. Amsterdam: Elsevier.
Strolin Benedetti M, Dostert P (1989) Monoamine oxidase, brain ageing and degenerative diseases. Biochem Pharmacol 38:555–561.
Strolin Benedetti M, Kaene PE (1980) Differential changes in MAO-A and -B activity in the aging rat brain. J Neurochem 35:1026–1032.
Tago H, Kimura H, Kitahama K, Sakai K, Jouvet M, Maeda T (1984) Cortical projections of monoamine oxidase-containing neurons from the posterior hypothalamus in the rat. Neurosci Lett 52:281–286.
Tago H, Reiner PB, McGeer EG (1987) Coupled intracellular horseradish peroxidase-monoamine oxidase histochemistry: description of the technique and its application to the study of physiologically identified tuberomammillary neurons. J Neurosci Methods 20:271–281.

Tetrud JW, Langston JW (1989) The effect of deprenyl (selegiline) on the natural history of Parkinson's disease. Science 245:519–522.
Thorpe LW, Westlund KN, Kochersperger LM, Abell CW, Denney RM (1987) Immunocytochemical localization of MAO-A and -B in human peripheral tissues and brain. J Histochem Cytochem 35:23–32.
Trendelenburg U (1990) The interaction of transport mechanisms and intracellular enzymes in metabolizing systems. J Neural Transm [Suppl] 32:3–18.
Waldmeier PC, Delini-Stula A, Maître L (1976) Preferential deamination of dopamine by an A type monoamine oxidase in rat brain. Naunyn Schmiedebergs Arch Pharmacol 292:9–14.
Westlund KN, Denney RM, Kochsperger LM, Rose RM, Abell CW (1985) Distinct MAO A and MAO B populations in the primate brain. Science 230:181–183.
Westlund KN, Denney RM, Rose RM, Abell CW (1988) Localization of distinct monoamine oxidase A and monoamine oxidase B cell populations in human brainstem. Neuroscience 25:439–456.
Willoughby J, Glover V, Sandler M (1988) Histochemical localisation of MAO-A and -B in rat brain. J Neural Transm 74:29–42.
Yoo BY, Oreland L, Persson A (1974) Effect of formaldehyde and glutaraldehyde fixation on the monoamine oxidase activity in isolated rat liver mitochondria. J Histochem Cytochem 22:445–446.
Youdim MBH, Finberg JPM (1990) New directions in monoamine oxidase A and B: selective inhibitors and substrates. Biochem Pharmacol 41:155–162.
Youdim MBH, Finberg JPM, Tipton KF (1988) Monoamine oxidase. In: Handbook of experimental pharmacology, Vol 90/1, Catecholamines, I (Trendelenburg U, Weiner N, eds), pp 119–192. Berlin: Springer.